UNIVERSITY OF CALIFORNIA SAN DIEGO

SAN DIEGO STATE UNIVERSITY

Evaluation of Metabolic Dehydrogenases in Cancer

A dissertation submitted in partial satisfaction of the
requirements for the degree

Doctor of Philosophy

in

Biology

by

Joi LaGrace Weeks

Committee in charge:

University of California San Diego

Professor Gen-Sheng Feng
Professor Shannon Lauberth

San Diego State University

Professor Christal Sohl, Co-Chair
Professor Ricardo Zayas, Co-Chair
Professor Erica Forsberg
Professor Carrie House

2020

The Dissertation of Joi LaGrace Weeks is approved, and it is acceptable in quality and form for publication on microfilm and electronically:

Co-Chair

Co-Chair

University of California San Diego

San Diego State University

2020

DEDICATION

I would like to dedicate this dissertation to my late grandfather, Lee Ernest Perry, Sr., who never had the opportunity to further his education, but made sure that his children and grandchildren did. You taught me the value of hard work by hand, humility and limitless creativity. You kindled my need and enjoyment in engineering solutions to problems and unravelling complexity to make things simple. I am who I am because of your faith in me.

I also dedicate this dissertation to my mother, Mattie Perry-Johnson, husband, Robert Kirk Griffin and children, Sun and Trinity Griffin. Mom, thank you for strengthening your weaknesses in me, science and math are enjoyable because you placed me in Math in Science programs all through grade school because you couldn't teach me. That fed my desire to use them both daily, as a scientist. Kirk, thank you for your patience and support during the rough and smooth times during my pursuit for a Ph.D. It's amazing that we're still together though all that went down. Sun and Trinity, you both can do anything you put your mind to. Do not sell yourselves short. Just find the fire of motivation and determination within yourselves and use it to accomplish the impossible, because nothing is truly impossible.

TABLE OF CONTENTS

LIST OF ABBREVIATIONS

1,3 BPG	1,3-diphosphoglycerate
293T	Human embryonic kidney cells
Å	Angstroms
Ac-CoA	Acetyl coenzyme A
ACACA	Ac-CoA carboxylase 1
αKG	alpha-ketoglutarate
AMP	Adenosine monophosphate
Asp	Aspartate
ATP	Adenosine triphosphate
Cit	Citrate
D	Aspartic Acid
D2HG	D-2-dehydroxyglutarate
DE3	gamma-DE3 lysogen
De novo	Anew
DTT	Dithiothreitol
DMSO	Dimethyl sulfoxide
FASN	Fatty acid synthase
FBS	Fetal Bovine Serum
FLAG	Polypeptide protein tag

Fum	Fumarate
G418	Geneticin
GAP	Glyceraldehyde-3-phosphate
GAPDH	Glyceraldehyde-3-phosphate dehydrogenase
GC-MS	Gas chromatography-mass spectrometry
Glc	Glucose
Glu	Glutamate
GLUT1	Glucose transporter 1
Gln	Glutamine
H	Histidine
H1792	NCI-1792 adenocarcinoma NSCLC cells
H520	NCI-H520 squamous carcinoma NSCLC cells
H520 MDH1^{+}	Amplified MDH1 H520 clonal line
Holo	Protein bound with its substrates and cofactors
IDH	Isocitrate dehydrogenase
In vitro	In cell culture (outside an organism)
K	Lysine
K-to-G	Lysine mutated to glutamine
KAT	Lysine acetyltransferases
k_{cat}	Rate constant describing the maximal steady-state rate

K_M	Michaelis-Menten rate constant
k_{obs}	Observed rate
KO	Knock out
L	Leucine
LDHA	Lactate dehydrogenase
Lys	Lysine
M#	Number of isotopes per molecule
Mal	Malate
MDH	Malate dehydrogenase
ME1	Malic enzyme 1
$MgCl_2$	Magnesium chloride
NAD(H)	Nicotinamide adenine dinucleotide
NADP(H)	Nicotinamide adenine dinucleotide phosphate
NaCl	Sodium chloride
NSCLC	Non-small cell lung cancer
NuLi-1	Normal lung epithelial airway cell line
OAA	Oxaloacetate
OD	Optical density
PDB	Protein database
PTM	post-translational modification

Pyr	Pyruvate
Q	Glutamine
R	Arginine
S	Serine or Ser
SIRT	Sirtuin
Suc	Succinate
TCA	Tricarboxylic acid
tRNA	Transfer RNA
WT	Wild Type
Y	Tyrosine

LIST OF FIGURES

LIST OF TABLES

ACKNOWLEDGMENTS

Initially, I would like to express my gratitude to my mentor, Dr. Christal D. Sohl. Without you, I wouldn't have a lab to work in or dissertation to defend. Thank you for your support and guidance. I dreamed of having a mentor that is passionate about science and teaching the next generation, who's human and lets me also be human while I grow as a scientist and doesn't forget the struggles of those they are guiding. I'm lucky to have found such an intelligent, caring, joyful, passionate scientist to learn from. I didn't think you existed, and I'm honored to know that you do and to have worked with you. Older more established principle investigators could learn a thing or two from you about mentoring, which is a refreshing thought since you're so early on in your career.

I would like to thank my committee members, Drs. Christal Sohl, Ricardo Zayas, Shannon Lauberth, Gen-Sheng Feng, Carrie House, and Erica Forsberg. You all joined my committee after I advanced to candidacy and were still willing to offer me your guidance and unmeasurable expertise. I'm so grateful for you all and my words will never fully express how much I appreciate all of you.

I would like to acknowledge the Ford Foundation, ARCS, University of California San Diego Graduate Department, and the U54 for your financial help of my research. Without your support, I would have been without a lab and stiped during my transition, but thankfully I didn't have to worry about my finances at that time because of you. Additionally, thank you to the San Diego State Biology Department and Joint-Doctoral Program for facilitating my growth as a scientist. Thank you to Drs. Cathie Atkins, Joe Pogliano, Ricardo Zayas, Estralita Martin and Aaron I. Bruce for helping me in my transition to the Sohl lab and at times in the aftermath.

I would like to acknowledge all of the Sohlmates that I have encountered and worked with in the Sohl lab. Thank you for making our lab an enjoyable place to work. I've learned so much from you all about enzymes, pop culture, and even about the future goals that you all are working to reach. Keep going and do not give up. Specifically, I would like to thank Diego Matteo, Lucas Luna, An Huang, and Grace Wells for helping me become quickly established in the lab and for accepting me as a fellow colleague. Thank you to my undergrads Sati Alexander, Alexandria Strom, Vinnie Widjaja and Dahra Pucher for all of your work with cell culture and/or protein purification plus kinetics. We've repeated so many of the purifications and kinetic analysis for the WT IDH1 K-to-Q mutants that I can now dub you "experts in WT IDH1 K-to-Q kinetics." Thank you to the Sussmaniacs from my previous lab for all of your help in my previous project that I will not discuss in this document. Specifically, I'd like to thank Drs. Roberto Alverez Jr., Jessica Wang, and Natalie Gude for your scientific and emotional support, especially during my transition and once I joined the Sohl lab.

Chapter 1, in full, is currently in preparation for publication. (Tentative Title) Understanding IDH1 regulation through site-specific acetylation mimics. Joi Weeks, Alexandra Strom, Vinnie Widjaja, Sati Alexander, Dahra Pucher, and Christal D. Sohl. The dissertation author will be the primary researcher and author of this paper.

VITA

Education

San Diego State University & University of California San Diego, California
Doctor of Philosophy in Cell and Molecular Biology June 2020

San Diego State University, San Diego, California
Master of Science in Cell and Molecular Biology December 2015

University of North Carolina at Chapel Hill, Chapel Hill, North Carolina
Bachelor of Science in Chemistry May 2007

Publications

Joi Weeks, Alexandra Strom, Vinnie Widjaja, Sati Alexander, Dahra Pucher, and Christal D. Sohl. *Understanding IDH1 regulation through site-specific acetylation mimics.* (In preparation)

Bingyan J. Wang, Roberto Alvarez Jr, Alvin Muliono, Sharon Sengphanith, Megan M. Monsanto, **Joi Weeks**, Roberto Sacripanti, and Mark A. Sussman. *Adaptation within embryonic and neonatal heart environment reveals alternative fates for adult c-kit+ cardiac interstitial cells*. Stem Cells Transl Med. 2019; 9(5):620-635. doi: 10.1002/sctm.19-0277.

Ching-Hsin Huang, Natalie Mendez, Oscar Hernandez Echeagaray, **Joi Weeks**, James Wang, Charles Vallez, Natalie Gude, William Trogler, Dennis Carson, Tomoko Hayashi, and Andrew C. Kummel. *Conjugation of a small molecule TLR7 agonist to silica nanoshells enhances adjuvant activity.* ACS Appl Mater Interfaces. 2019;11(30):26637-26647. doi: 10.1021/acsami.9b08295.

James Wang, Christopher V. Barback, Casey N. Ta, **Joi Weeks**, Natalie Gude, Robert F. Mattrey, Sarah L. Blair, William C. Trogler, Hotaik Lee, and Andrew C. Kummel. *Extended lifetime* in vivo *pulse stimulated ultrasound imaging.* IEEE Trans Med Imaging. 2018;37(1):222-229. doi: 10.1109/tmi.2017.2740784.

Claire S. Koechlein, Jeffery R. Harris, Timothy K. Lee, **Joi Weeks**, Ray G. Fox, Brian Zimdahl, Ito T, Allen Blevins, Seung-Hye Jung, John P. Chute, Amit Chourasia, Markus W. Covert, and Tannishtha Reya. *High-resolution imaging and computational analysis of haematopoietic cell dynamics* in vivo*.* Nat Commun. 2016; 7:12169. doi:10.1038/ncomms12169.

Jordana M. Henderson, Sean V. Nisperos, **Joi Weeks**, Mahjoobah Ghulam, Ignacio Marín, and Ricardo M. Zayas. *Identification of HECT E3 ubiquitin ligase family genes involved in stem cell regulation and regeneration in planarians.* Dev. Biol. 2015;404(2):21-34. doi: 10.1016/j.ydbio.2015.04.021.

Hyog Young Kwon, Jeevisha Bajaj, Takahiro Ito, Allen Blevins, Takaaki Konuma, **Joi Weeks**, Nikki K. Lytle, Claire S. Koechlein, David Rizzieri, Charles Chuah, Vivian G. Oehler, Roman Sasik, Gary Hardiman, and Tannishtha Reya. *Tetraspanin 3 Is required for the development and propagation of acute myelogenous leukemia.* Cell Stem Cell. 2015;17(2):152-164. doi.org/10.1016/j.stem.2015.06.006.

Bryan Zimdahl, Takahiro Ito, Allen Blevins, Jeevisha Bajaj, Takaaki Konuma, **Joi Weeks**, Claire S Koechlein, Hyog Young Kwon, Omead Arami, David Rizzieri, H Elizabeth Broome, Charles Chuah, Vivian G Oehler, Roman Sasik, Gary Hardiman and Tannishtha Reya*. Lis1 regulates asymmetric division in hematopoietic stem cells in leukemia.* Nat Genet. 2014 ;46(3):245-52. doi:10.1038/ng.2889.

Honors & Awards

2017-2020	*ARCS Scholarship*, San Diego State University
2017-2020	*Ford Foundation Scholarship*, National Academy of Sciences
2016	*San Diego Fellowship*, University of California San Diego
2014	*Harold and June Grant Memorial Scholarship*, San Diego State University
2012	*Graduate School Scholarship*, Black Opal/Biocosmetic Research Labs

Professional Presentations

Joi Weeks, Alexandra Strom, Vinnie Widjaja, Sati Alexander, Dahra Pucher, Christal D. Sohl. *Understanding IDH1 regulation through site-specific acetylation mimics.* Poster. SDSU Student Research Symposium (SRS) 2020.

Joi Weeks, Grace Wells, Sati Alexander, Christian Metallo, Christal D. Sohl. *Investigating the reversible MDH1 catalytic reaction in squamous non-small cell lung cancer.* Poster. American Association of Cancer Research 2019.

Joi Weeks, Grace Wells, Sati Alexander, Christian Metallo, Christal D. Sohl. *Modulating the reversible MDH1 catalytic reaction in squamous non-small cell lung cancer.* Poster. SDSU SRS 2019.

Joi Weeks, Oscar Echeagaray, Natalie Mendez, James Wang, Nick Vallez, Natalie Gude, Andrew Kummel. *Investigating the use of Toll-like receptor 7 ligand bound nanoshells for immune activation*. Poster. Ford Foundation 2018.

Joi Weeks, Natalie Mendez, Oscar Hernandez Echeagaray, Ching-Hsin Huang, Stephen Calderon, Charles Vallez, Adrian Badaracco, Tomoko Hayashi, Dennis Carson, Natalie

Gude, Andrew Kummel. *Nanoshells enabled tumor ablation in combination with immunotherapy*. Poster. U54 Progress 2017.

Joi Weeks, Jordana Henderson, Sean Nisperos, Maji Ghulam, Ignacio Martin, Ricardo Zayas. *Identification of E3 ubiquitin ligase genes in stem cell regulation*. Poster. CMB Graduate Student Symposium 2015.

Joi Weeks, Jordana Henderson, Maji Ghulam, Sean Nisperos, Ignacio Martin, Ricardo Zayas. *Identification of HECT E3 ubiquitin ligases involved in regulating regeneration in planarians*. Poster. Society for Developmental Biology 2014.

Professional Experience

Biology and Chemistry/Biochemistry Departments, San Diego State University & University of California San Diego, San Diego 2018-Present

Joint Ph.D. Program Graduate Student in Dr. Christal Sohl's lab investigating the chemical and cellular characteristics required to drive MDH1 catalysis in non-small-cell lung cancer, and molecular mechanisms of regulation of IDH1.

Biology Department, San Diego State University & University of California San Diego, San Diego 2015-2018

Joint Ph.D. Program Graduate Student in Drs. Natalie Gude's and Mark Sussman’s lab investigating the effect of TLR7 agonist conjugated nanoparticles in educating the immune system about cancer and tumor metastasis in collaboration with Drs. Andy Kummel, Tomoko Hayashi and Dennis Carson at UCSD.

Biology Department, San Diego State University, San Diego 2014-2016

Teaching Associate for Biology 366L, Upper level Cell and Molecular Biology. Prepared and presented lectures on cell separation and fragmentation, cloning, microscopy, bioinformatics, restriction mapping, etc. Developed quizzes, graded assignments, proctored and resolved questions.

Biology Department, San Diego State University, San Diego 2013-2015

Cell and Molecular Biology Master's Student in Dr. Ricardo Zayas' lab exploring the role of E3 ubiquitin ligases in adult stem cell regulation and differentiation in *S. Mediterranea* and investigating the mechanisms underlying adult stem cell differentiation downstream of Ndk.

Pharmacology Department, University of California, San Diego California 2011-2013

Staff Research Associate II in Dr. Tannistha Reya's Lab investigating signals that drive hematopoietic stem cell self-renewal and differentiation during regeneration and dysregulation.

Pharmacology Department, Duke University, Durham North Carolina 2010

Laboratory Technician in Dr. Tannishtha Reya's Lab investigating high resolution imaging in the context of hematopoietic stem cells using mouse models.

Wyeth Biotech, Sanford North Carolina 2007-2008

Quality Control Laboratory Technician for the Data & Sample Management Department of a child vaccine manufacturer.

Genetics Department, University of North Carolina at Chapel Hill 2004-2005

Laboratory Assistant in Dr. David Threadgill's Lab investigating the role of the Epidermal Growth Factor Receptor (Egfr) using mouse models.

ABSTRACT OF DISSERTATION

Evaluation of PTM Regulation and Enzymatic Catalysis in Cancer

by

Joi LaGrace Weeks

Doctor of Philosophy in Biology

University of California, San Diego, 2020

San Diego State University, 2020

Assistant Professor Christal D. Sohl, Co-Chair

Professor Ricardo Zayas, Co-Chair

Cancer cells can reprogram their metabolism through altering metabolic enzymes to support increased lipid synthesis, cell proliferation, glycolysis, and tricarboxylic acid (TCA) cycling. Two important cytosolic enzymes that play a role in driving these processes include isocitrate dehydrogenase 1 (IDH1) and malate dehydrogenase 1 (MDH1), though details of their regulation and their role in cancer is still under exploration. IDH1 catalyzes the reversible conversion of isocitrate to α-ketoglutarate (αKG) via $NADP^+$-dependent oxidation in the cytosol and in peroxisomes of cells. Mutations primarily at residue R132 have been identified in low grade gliomas and secondary glioblastomas, causing the neomorphic production of D-2-dehydroxyglutarate (D2HG) from αKG coupled to NADPH oxidation. Little is currently known about how human IDH1 activity is regulated, though recent proteomics data identified lysine acetylation sites in WT IDH1. We created lysine to glutamine (K-to-Q) acetylation mimics (Lys81, Lys224, Lys321) in WT and R132H IDH1, and found that acetylation inhibits WT IDH1 and variably regulates R132H IDH1 catalysis. A second metabolic dehydrogenase implicated in cancer is MDH1, an enzyme critical for replenishing cytosolic metabolites and for driving glycolysis through the production of NAD^+ and malate from NADH and oxaloacetate (OAA), respectively. MDH1 has been reported to be amplified in squamous cell non-small cell lung cancer (NSCLC), which has high glycolytic activity. Elucidation of the role of MDH1 in altering cellular metabolism to drive tumorigenic progression has yet to be determined. Thus, we evaluated the metabolomic features in our MDH1 models and determined that loss of MDH1 led to decreased proliferation, TCA cycling, lactate secretion, and lipogenesis. We also found that amplification of MDH1 caused increased expression of malic enzyme 1 (ME1) in MDH1 amplified cell line.

CHAPTER 1

Investigating IDH1 Regulation through Site-Specific Acetylation Mimics

INTRODUCTION

Isocitrate dehydrogenase 1 (IDH1) is a homodimeric enzyme that catalyzes the $NADP^+$-dependent conversion of isocitrate to α-ketoglutarate (αKG) in the cytoplasm and peroxisomes (Fig. 1a). IDH1, along with mitochondrial IDH2 ($NADP^+$) and IDH3 (NAD^+), is a member of the IDH family of enzymes that generate important metabolites and reducing equivalents needed for fatty acid synthesis and oxidative metabolism. Two family members, IDH1 and IDH2, can deleteriously acquire mutations that alter the normal reaction. IDH1 point mutations, primarily R132H, drive > 80% of lower grade gliomas and secondary glioblastomas by catalyzing the neomorphic production of the oncometabolite D-2-hydroxyglutarate (D2HG) from αKG in an NADPH-dependent reaction [3-5] (Fig. 1b). D2HG can inhibit αKG-dependent enzymes such as DNA and histone demethylases, leading to genome hypermethylation and cell de-differentiation [6,7]. Mutant IDH1 has been successfully targeted therapeutically, with an FDA-approved selective inhibitor currently in the clinic [8]. Wild type (WT) IDH1 has also been implicated in cancer [9-11].

Though mutant and WT IDH1 activity implicated in tumor growth and formation has been characterized biochemically [9,12-14], less is known about how human IDH1 is regulated. While IDH1 is conserved across many species such as yeast, bacteria, fish and mice, mechanisms of regulation appear to be divergent [1,15,16]. For example, yeast is allosterically regulated by AMP; following isocitrate binding, allosteric association of AMP causes increased isocitrate affinity. In contrast, human IDH1 doesn't appear to have an AMP binding site [1]. In bacteria, IDH is phosphorylated at residue S113, found near the active site, to halt enzyme activity [1,15,16]. While this residue is structurally conserved in human IDH1 (S94), this residue does not appear to be phosphorylated in

humans. Instead, D279 hydrogen bonds with S94 to mimic the structural consequences of serine phosphorylation [1,15,17]. However, phosphorylation may still prove to be important for IDH1 regulation; it has recently been reported that phosphorylation at Y42 and Y391 are important for cofactor binding and IDH1 dimerization, respectfully [18].

Protein acetylation is a common strategy used by eukaryotes to alter protein structure and function. Addition of acetyl groups to lysines are catalyzed by lysine acetyltransferases (KATs). However, there is evidence that this reaction may also occur non-enzymatically, primarily in the mitochondria [19]. While protein acetylation is most commonly associated with the regulation of histones, many cytosolic [20-24] and metabolic [24-26] enzymes are also regulated by this post-translational modification (PTM). For example, IDH2, which has high sequence and structural homology to IDH1, is regulated via acetylation [27,28]. Once acetylated at K413, IDH2 loses activity by ~44-fold, though the deacetylase SIRT3 can restore this activity through removal of the acetyl group under calorie and glucose restriction in mice [27]. The catalytic consequences of K413 and K256 acetylation in IDH2 were also studied using lysine to glutamine (K-to-Q) mutants *in vitro*, and acetylation of both residues inhibited catalysis [28].

Several proteomic data sets show that several lysines in IDH1 are acetylated, including K81, K224 and K321 [29-31]. All three lysines are located near but not in the active site of IDH1. K224 and K321 are conserved in IDH2, but K81 is not. Recently, K224 acetylation in IDH1 was investigated in colon cancer and found to have an inhibitory role, though the consequences K81 and K321 acetylation in IDH1 have yet to be explored. Here, we investigate the effects of acetylation on IDH1 activity by measuring steady-state kinetic parameters of K-to-Q mimics in WT and R132H IDH1 backgrounds. We show that

WT IDH1 mimics are inhibited, while R132H IDH1 mimics have more complex consequences. Overall, our work supports the growing evidence that IDH1 is regulated by lysine acetylation.

MATERIALS AND METHODS

Materials

Tris–hydrochloride, sodium chloride, magnesium chloride hexahydrate, and α-ketoglutarate (αKG, sodium salt) were purchased from Fisher (Hampton, NH). The pH of αKG stocks was adjusted to 7.0 before use. *DL*-isocitric acid trisodium salt hydrate and coenzyme A trilithium salt dihydrate (Acetyl-CoA) was purchased from MP Biomedicals (Santa Ana, CA). NADPH (tetrasodium salt) and $NADP^+$ (disodium salt) were purchased from Calbiochem (San Diego, CA). Dimethyl sulfoxide (DMSO) and lithium potassium acetyl phosphate (acetyl-phosphate) were purchased from Sigma–Aldrich (St. Louis, MO). Bovine serum albumin (BSA) was purchased from SeraCare Lifescience (Milford, MA).

Plasmid Mutagenesis

All WT IDH1 and R132H IDH1 mutant constructs were in a pET-28b vector containing an *N*-terminal hexahistidine tag. Site-directed mutagenesis (Kapa Biosciences, Wilmington, MA) was used to generate K81Q (forward primer, 5'- GCC ACC ATT ACA CCG GAT GAA CAG CGT GTG GAA GAA TTT AAA C -3', reverse primer, 5'- GTT TAA ATT CTT CCA CAC GCT GTT CAT CCG GTG TAA TGG TGG C -3'); K224Q (forward primer, 5'- CCA TTC TGA AAA AAT ACG ATG GTC GCT TTC AGG ATA TTT TTC AAG AAA TTT ACG ATA AAC -3', reverse primer, 5'- GTT TAT CGT AAA TTT CTT GAA AAA TAT CCT GAA AGC GAC CAT CGT ATT TTT TCA GAA TGG -3'); K321Q (forward primer, 5'- CGT CAT TAT CGT ATG TAT CAG CAG GGT CAA GAA ACC AGC ACC AAT -3', reverse primer, 5'- ATT GGT GCT GGT TTC TTG ACC CTG CTG ATA CAT ACG ATA ATG ACG -3'); and D79L (forward primer, 5'- GTT AAA TGC GCC ACC

ATT ACA CCG CTG GAA AAA CGT GTG GAA GAA TTT AAA-3', reverse primer, 5'- TTT AAA TTC TTC CAC ACG TTT TTC CAG CGG TGT AAT GGT GGC GCA TTT AAC -3'). All constructs were confirmed by sequencing.

Protein Purification

All WT IDH1 and R132H IDH1 mutant proteins were expressed and purified using conditions published previously [5,32]. Briefly, BL21 gold (DE3) cells were transformed with an IDH1 construct until an OD_{600} of 1.0–1.2 was reached. The temperature was reduced to 18 ^{o}C and expression was induced with a final concentration of 1 mM isopropyl β-D-1-thiogalactopyranoside followed by 18–20 h incubation. The protein lysate was purified using nickel-nitrilotriacetic acid column chromatography (Qiagen, Valencia, CA) and dialyzed in storage buffer (50mM Tris pH 7.5 at 4oC, 100mM NaCl, 20% glycerol, 1mM DTT). Purity (≥ 90%) was confirmed by SDS-PAGE, and IDH1 was flash frozen in liquid nitrogen and stored at 80 °C for no longer than 1.5 months.

Steady-State Activity Assays

An 8452 diode array spectrophotometer was used (OLIS, Atlanta, GA) for all enzymatic assays. Enzymatic concentrations were optimized for each protein to ensure optimal signal and linear range. For the conversion of isocitrate to αKG [5], the reaction was initiated by adding saturating concentrations of $NADP^+$ (200 μM final concentration) and varying concentrations of isocitrate to limiting concentrations of IDH1 protein (100 nM for K81Q, K224Q, K321Q IDH1 and 21 μM for D79L IDH1) in IDH1 assay buffer (50 mM Tris at 4^{o}C, pH 7.5 at 37 °C, 150 mM NaCl, 10 mM $MgCl_2$, 1 mM dithiothreitol). For the neomorphic conversion of αKG to D2HG [5], the reaction was initiated by adding

saturating concentrations of NADPH (200 μM final concentration) and varying concentrations of αKG to limiting concentrations of the R132H IDH1 double mutants (R132H/K81Q, R132H/K224Q, and R132H/K321Q IDH1, 500 nM) in assay buffer. The change in absorbance due to NADPH formation or depletion was monitored at 340 nm. For both reactions, the slope of the linear range of the incubations were calculated and converted to nM NADPH using the molar extinction coefficient for NADPH of 6.22 cm^{-1} mM^{-1} to obtain k_{obs} (*i.e.* nM NADPH/nM enzyme s^{-1} at each concentration of substrate). Results were fit to hyperbolic plots in GraphPad Prism (GraphPad Software, La Jolla, CA) to estimate k_{cat} and K_m mean values $\pm$ S.E. Assays were performed with at least two protein preparations.

RESULTS

K-to-Q IDH1 mutation results in inhibited activity

We used K-to-Q acetylation mimics as a proxy to better understand the consequences of acetylation on WT and R132H IDH1 activity. Previously reported mass spectrometry data sets from human, mouse and rat samples showed lysine positions K81, K87, K115, K224, K233, K243, and K321 were acetylated in WT IDH1 [29-31]. When evaluating these lysine sequence positions in human IDH1 and human IDH2 using the uniprot alignment tool [33], we found that K81 in IDH1 was not conserved in IDH2, but K87, K115, K224, K233, K243, and K321 were conserved in IDH2. It has previously been shown that acetylation of K256 and K413 in IDH2 inhibits activity [27,28], so we also noted that K256 IDH2 (K217 in IDH1) and K413 IDH2 (K374 in IDH1) were conserved in IDH1. However, there was no evidence of acetylation of these residues in IDH1 in the proteomic data [29-31].

Previous studies have shown that acetylation of lysines in or near the active site can affect substrate binding [34-36] or cause conformational changes that affect rates of catalysis [28,35,37]. Thus, acetylated lysines near the IDH1 active site (K81, K224, and K321) were prioritized to be probed using site-directed mutagenesis [29,31]. Of note, K224 IDH1 is structurally proximal to K256 in IDH2 (corresponding to K217 in IDH1), a lysine whose acetylation leads to inhibited IDH2 catalysis [28], and so we expected that mimicking acetylation at K224 in IDH1 would also confer inhibition. Distances of K81, K224, and K321 to the nearest substrate ($NADP^+$) in a previously solved crystal structure of holo IDH1 (PDB 1T09 [1]) were found to be similar distances away (~10 Å), though K321 was a bit more distant (13.7 Å, Fig. 2a). In a structure of holo R132H IDH1 (PDB

4KZO [2]), K81/R132H IDH1 was positioned ~2 Å farther away from NADPH when compared to K321/R132H and K224/R132H IDH1 (Fig. 2b).

Acetylation mimics (K81Q, K224Q and K321Q IDH1) were created using site-directed mutagenesis in WT and R132H IDH1 backgrounds. This strategy has been successful for elucidating the catalytic and structural consequences of lysine acetylation for a host of proteins such as IDH2, malate dehydrogenase, and histone H3 [19,28,38-40]. Steady-state experiments [5,15,28] probing the rates of αKG production were measured, and we found that K81Q IDH1 had a similar k_{cat} to WT IDH1, while K224Q and K321Q IDH1 had k_{cat} values reduced by > 80% (Fig. 2 and Table 1). All of the K-to-Q IDH1 mimics had similar K_M values, which were 5-fold higher than observed for WT IDH1 (Table 1). Thus, the catalytic efficiency of the IDH1 mimics decreased ~5-fold for K81Q IDH1 and ~8-fold for both K224Q and K321Q IDH1, driven primarily through a decrease in k_{cat} (Fig. 2 and Table 1). These results indicate that mimicking acetylation at residues K81, K224, and K321 in IDH1 leads to decreased αKG production.

K-to-Q R132H IDH1 mutants are both inhibited and activated

Changes in WT IDH1 activity upon mimicking lysine acetylation led us to evaluate if lysines in a R132H IDH1 background have similar effects on catalysis. R132H IDH1 is the most common point mutant found in IDH1 tumors and this mutant catalyzes the neomorphic reaction of D2HG production from αKG [3]. Double mutants (R132H/K81Q, R132H/K224Q and R132H/K321Q IDH1) were generated and assessed using steady-state kinetic assays designed to measure rates of D2HG production. Only modest changes in k_{cat} and K_M values were observed in the double mutants as compared to R132H IDH1 (Fig. 3 and Table 1). Mutations at residues K81Q/R132H and K224Q/R132H

IDH1 had the largest impact, with a 2-fold increase (K81Q/R132H IDH1) or decrease (K224Q/R132H IDH1) in catalytic efficiency that was driven primarily through an increase in K_m. We concluded that acetylation of R132H IDH1 can have modest yet complex consequences on catalysis.

Changes to residue D79 confirms the importance of the location of K224 in IDH1

Due to the location and positioning of K217 IDH1 near the active site, we were interested in testing the mechanistic consequences of the K224Q mutation in IDH1 [28]. Of the three lysines studied in this work, only K224 appeared near enough to other residues to engage directly in noncovalent interactions. Specifically, K224, located in helix **α**7 in IDH1, is 3 Å away from D79', which is located in helix **α**4 [1]. The proximity and orientation of these two residues suggest that these domains could be stabilized through a salt bridge interaction, and that this interaction could be disrupted upon acetylation of K224. Residues upstream from D79 help form part of the NADP(H) binding pocket [1], so stabilization of these domains could impact catalysis, though D79 itself is fairly distant from the active site (8.2 Å from $NADP^+$). To probe the importance of interactions between K224 and D79, we designed a D79 mutant that would destroy the potential for hydrogen bonding or salt bridge interactions with K224, but otherwise mimic the structure of an aspartic acid residue. Therefore, we generated, expressed, and purified D79L in WT IDH1 (Fig. 4d). Using steady-state kinetics, we determined that the k_{cat} of D79L IDH1 drastically decreased by > 99% to generate a catalytic efficiency that is 130-fold lower (Fig. 4d, Table 1). Detection of any activity by D79L IDH1 required a 21-fold increase in concentration of the enzyme. To our knowledge, this is the first time that D79 has been identified as being important to IDH1 catalysis.

DISCUSSION

In our experiments, we used K-to-Q mimics for K81, K224, and K321 in WT IDH1 and R132H IDH1. We found that acetylation has the potential to inhibit WT IDH1 and variably alter R132H IDH1 activity. An interesting future direction is to determine if simultaneous acetylation of lysines has an additive or synergistic effect. By designing K-to-Q mutations to occur in pairs or trios, the effect of acetylations simultaneously affecting several lysine residues could be mimicked. An example of the effects of additive PTMs has been seen in transcription factors and histones [41,42]. For example, acetylation and phosphorylation of the conserved regions of transcription factor FOXO3a affects other PTMs synergistically such as those in the forkhead domain [41]. Methylation and acetylation PTMs that compete for the same residue usually have opposing effects on gene expression in histones [42]. While there is no evidence of methylation at positions K81, K224 and K321 in IDH1, these sites have been reported to be ubiquitinated [29]. Thus, there is the potential for competition resulting in changes in enzymatic activity or stability of the protein. While acetylation mimics are valuable for understanding the potential kinetic consequences of lysine acetylation, one limit is that they cannot provide mechanistic information on the consequences of the PTM. Instead, systems biology methods in which acetylated lysines are incorporated during translation using N^{e}-acetyllysyl-tRNA synthetases/tRNAs are the gold standard to identify the global consequences of protein acetylation in cells [43] and represent an important future direction.

Our study focuses on the kinetic features of enzymatic activity of acetylation mimics in IDH1 WT and R132H IDH1, and we show biochemically that K321 and K81

also inhibit IDH1 WT activity. By also extending our work to evaluate acetylation in R132H IDH1, we now know that acetylation in this background is more complex, yielding both slight increases and decreases in activity depending on the affected lysine. However, it is unknown whether the effects seen in R132H IDH1 are strong enough to have physiological ramifications. Recently, K224 in IDH1 was found to be deacetylated by SIRT2 to inhibit colorectal cancer and liver metastases [44]. K224R IDH1 (deacetylation mimic) and K224Q IDH1 were stably expressed in 293T cells [44]. Our data confirms their finding that K224 acetylation inhibits IDH1 activity. They also evaluated the effects of K81 and K321 IDH2 by expressing deacetylation mimics in 293T cells, but the acetylation levels at these positions assessed by western were unchanged compared to WT IDH1 [44]. Therefore, no further evaluation was undertaken to determine if K81 and K321 acetylation contribute to slowing the progression of the cancer cells in their colorectal model.

Additionally, we sought to understand the structural consequences of lysine acetylation. Of the three lysine residues under investigation, K224 IDH1 appeared to have the greatest potential to noncovalently interact with a nearby residue (D79) via a salt bridge or hydrogen bonding. Mutation of D79 resulted in nearly full ablation of WT IDH1 activity, drastically overshadowing the changes seen by altering K224 and revealing the importance, and complexity, of this residue and its interactions in IDH1 activity.

Overall, we used steady-state kinetics to elucidate the catalytic consequences of lysines reported to be acetylated in IDH1 [29-31]. Kinetic parameters for a series of K-to-Q mimics, a valuable strategy for understanding the consequences of acetylation in vitro [19,28,35,38,40] were reported in both WT and R132H backgrounds. We show that

mimicked acetylation of 3 lysine residues (K81, K224 and K321) in IDH1 lead to inhibition in WT IDH1 and variably alter activity in R132H IDH1, suggesting that IDH1 acetylation may have a regulatory role. Acetylation of K224 IDH1 may affect a possible interaction with D79, a non-active site residue that we show is important for catalysis. Overall, this study provides a foundation for determining mechanistic consequences of IDH1 acetylation as a means of regulation.

TABLES

Table 1.1: Steady-state kinetics parameters for the reactions catalyzed by WT and R132H mutational variants.

k_{obs} rates were obtained for varying substrate concentrations from at least 2 protein preparations and to fit a hyperbolic function. The SE was determined by deviation from the hyperbolic fits.

IDH1	**k_{cat} (s^{-1})** **ICT → αKG**	**K_M (mM)** **ICT → αKG**	**k_{cat}/K_M ($mM^{-1}s^{-1}$)** **ICT → αKG**
WT	40.4 ± 0.8	$.03001 \pm 0.0008$	$1.3 \pm 0.1 \times 10^3$
K81Q	38 ± 1	0.14 ± 0.02	270 ± 40
K224Q	23.0 ± 0.8	0.14 ± 0.02	160 ± 20
K321Q	24 ± 1.0	0.14 ± 0.02	170 ± 20
D79L	0.315 ± 0.006	0.028 ± 0.003	10 ± 1
	k_{cat} (s^{-1}) **αKG → D2HG**	**K_M (mM)** **αKG → D2HG**	**k_{cat}/K_M ($mM^{-1}s^{-1}$)** **αKG → D2HG**
R132H	1.09 ± 0.02	0.51 ± 0.04	2.1 ± 0.2
R132H K81Q	1.26 ± 0.03	0.24 ± 0.03	5.2 ± 0.7
R132H K224Q	0.84 ± 0.02	1.0 ± 0.1	0.9 ± 0.1
R132H K321Q	0.91 ± 0.01	0.37 ± 0.02	2.5 ± 0.1

FIGURES

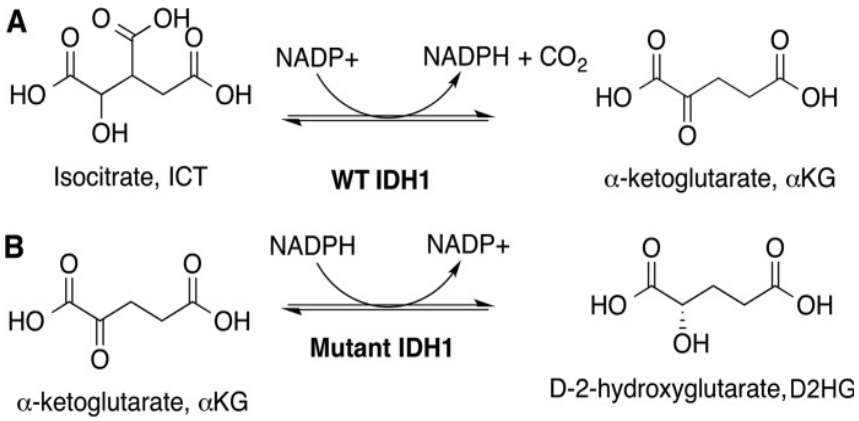

Figure 1.1: Reactions catalyzed by WT IDH1 and R132H IDH1 reactions

(A) WT IDH1 and (B) mutant IDH1 reactions.

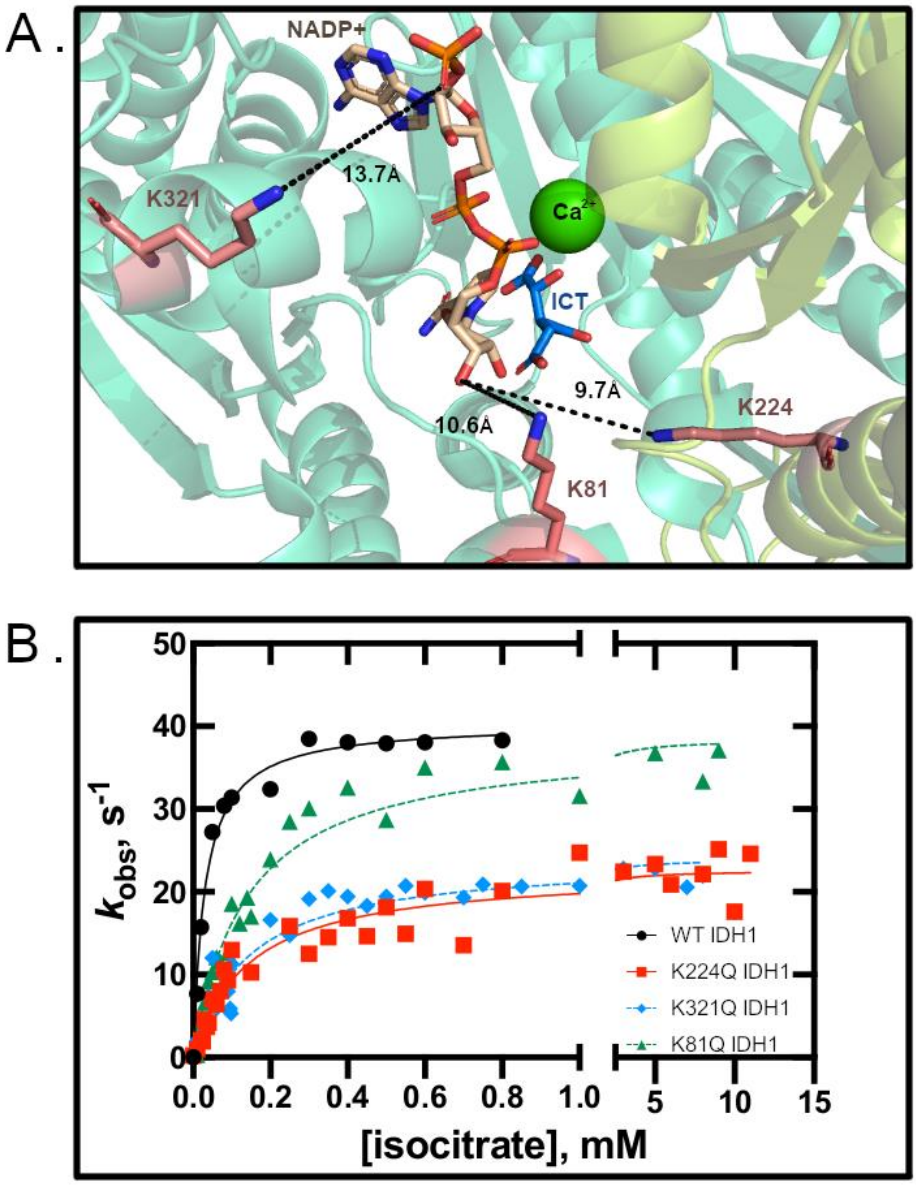

Figure 1.2: K224Q IDH1 inhibits IDH1 activity

(A) The active site of IDH1 with lysine residues shown in coral, and their distances from $NADP^+$ are shown in Å (PDB 1T09 [1]). (B) Overlaid Michaelis-Menten plots revealing differences in k_{cat} and K_M parameters among the mutants.

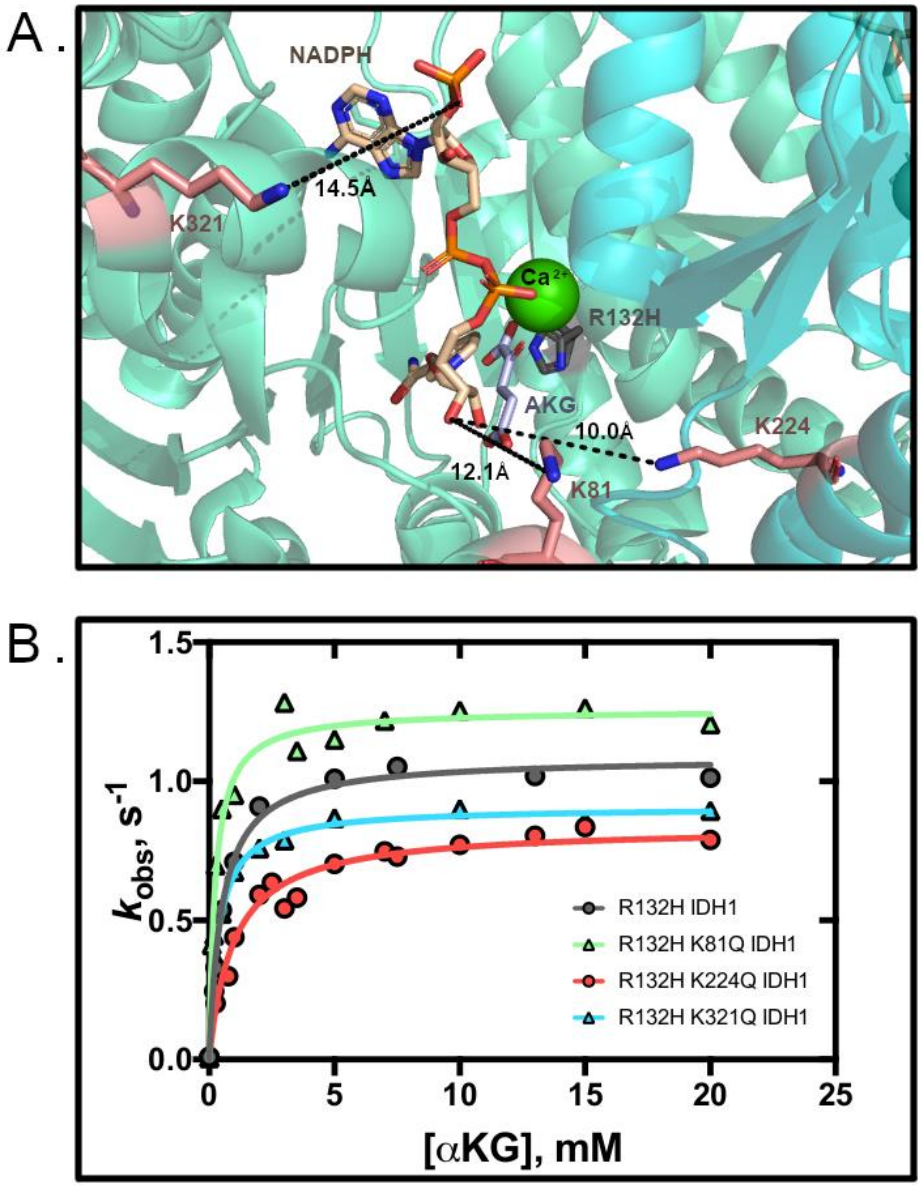

Figure 1.3: Acetylation mimics in R132H IDH1 lead to modest increased and decreased activity.

(A) The active site of R132H IDH1 with lysine residues identified in red and distances from NADPH are shown in in Å (PDB 4KZO [2]). (B) Overlaid Michaelis-Menten plots revealing differences in k_{cat} and K_M parameters.

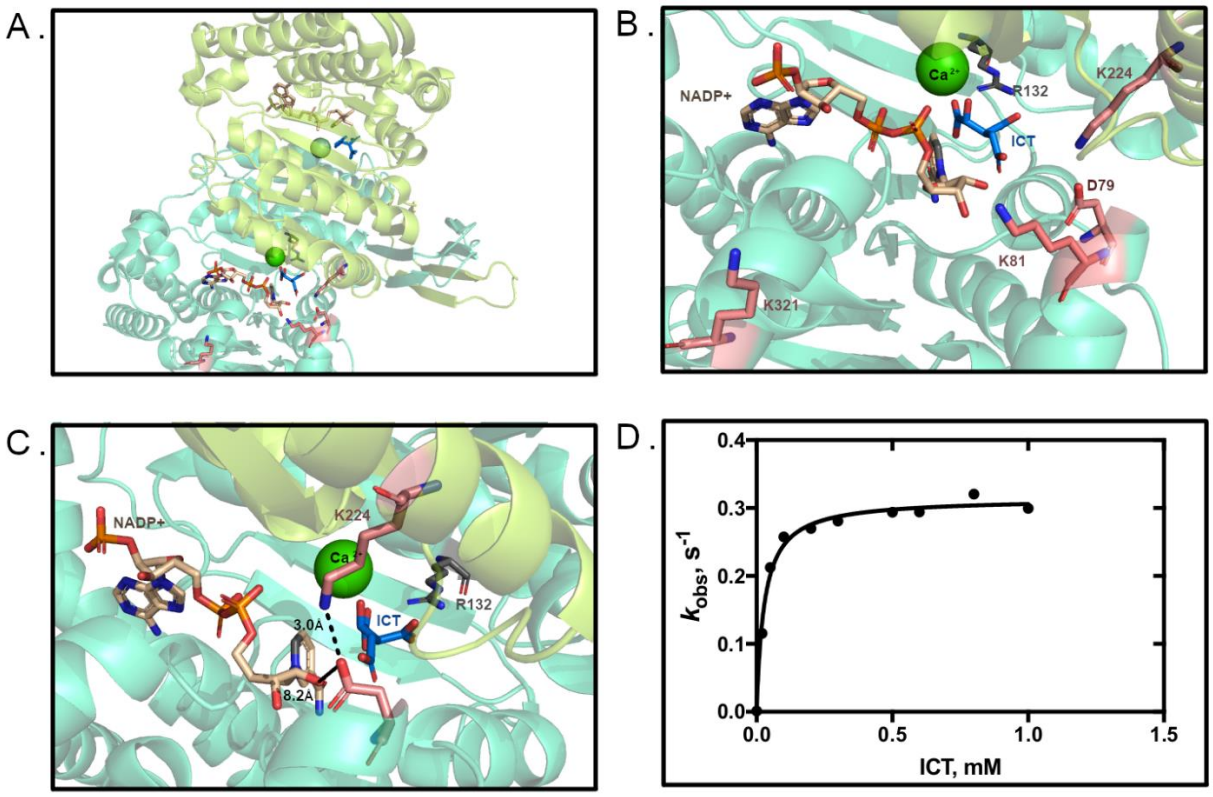

Figure 1.4: Mutation of D79, which is proximal to K224, ablates IDH1 activity

(A) IDH1 WT dimer (PDB 1T09 [1]). (B) Active site of IDH1 in the same orientation shown in A, with mutated residues and substrates indicated. (C) IDH1 active site, highlighting D79 and its distance to K224 and $NADP^+$. (D) Michaelis-Menten plot of D79L IDH1.

SUMMARY

Human IDH1 regulation is much less understood as compared to the study of regulatory strategies in other organisms such as bacteria. Previous IDH1 studies focused on the biochemical evaluation of WT and mutant IDH1 in tumors instead of determining how activity in IDH1 is regulated at the protein level. We undertook this study to determine the kinetic consequences of acetylation by creating K-to-Q mimics at K81, K224 and K321 in WT and R132H IDH1. We found that acetylation could lead to inhibition of WT and variable changes in R132H IDH1 activity. We advanced this study by also evaluating the K224 to D79 salt bridge interaction to find that D79 is highly critical for IDH1 activity, since alteration of this residue largely reduced IDH1 activity by more than 99%. Collectivity, our findings suggest that IDH1 is regulated by acetylation, supporting the idea that K224 is an important residue in IDH1. We also show that D79, which appears to interact with K224, also plays an important role in IDH1 catalysis.

Chapter 1, in full, is currently in preparation for publication. (Tentative Title) Understanding IDH1 regulation through site-specific acetylation mimics. Joi Weeks, Alexandra Strom, Vinnie Widjaja, Sati Alexander, Dahra Pucher, and Christal D. Sohl. The dissertation author will be the primary researcher and author of this paper.

CHAPTER 2

Understanding the catalytic consequences of MDH1 in NSCLC

INTRODUCTION

Lung cancer is the leading cause of cancer deaths world-wide and is classified into two groups: small cell lung cancer and non-small cell lung cancer (NSCLC). NSCLC, an aggressive form of cancer found in smokers and nonsmokers alike, is further subdivided into three groups based upon cell morphology: adenocarcinoma, squamous cell carcinoma, and large cell carcinoma. The two most common NSCLC subtypes are adenocarcinoma, a fast-growing tumor in alveoli, and squamous cell carcinoma, a slower growing tumor in the bronchi. Such differences in growth identify the potential differences in metabolic demand between these NSCLC subtypes.

MDH1, one of two malate dehydrogenase isoenzymes, is a cytoplasmic enzyme that generates NAD^+ equivalents for glycolysis as well as for the tricarboxylic (TCA) cycle through the malate aspartate shuttle. MDH1 reversibly catalyzes the NAD^+-dependent production of oxaloacetate (OAA) to malate. MDH1 has been reported to be amplified in squamous NSCLC, which is highly glycolytic [45]. Disease-free survival rates after ~3 years in squamous NSCLC patients drop from 35% to 0% in squamous NSCLC patients with amplified MDH1 [46]. Evaluating changes in MDH1 expression to determine alterations in cancer cell phenotype will help to reveal the role of MDH1 amplification in NSCLC.

Glycolysis is the process of converting glucose to pyruvate, which is ultimately used to generate the energy equivalent ATP. Such processing also generates nicotinamide adenine dinucleotide phosphate (NADPH) and acetyl coenzyme (Ac-CoA), which are critical for fatty acid synthesis as well as lactate secretion. In glycolysis, the conversion of glyceraldehyde-3-phosphate (GAP) to 1,3-diphosphoglycerate (1,3 BPG)

by glyceraldehyde-3-phosphate dehydrogenase (GAPDH) requires NAD^+, and if it is unavailable, glycolysis will not continue. Thus, MDH1 can directly support glycolysis by generating NAD^+ in the cytoplasm under aerobic conditions. Lactate dehydrogenase (LDHA) is also capable of generating NAD^+ by converting pyruvate to lactate under anaerobic conditions, however Otto Warburg found in 1926 that cancer cells consume large levels of glucose and convert it to lactate regardless of oxygen status [47].

De novo lipid synthesis requires glucose as its main substrate. Once glucose exits glycolysis as pyruvate, it enters the TCA cycle and exits as citrate to create an Ac-CoA pool in the cytoplasm reserved for lipogenesis. In cancer cells, glycolysis and glucose transporters have been shown to be upregulated by the PI3K/Akt/mTOR pathway [48,49]. For example, squamous NSCLC has been shown to be dependent on glucose through increased expression of glucose transporter 1 (GLUT1), which is not the case in adenocarcinomas [49]. Glucose increases lead to higher production of lactate and pyruvate that can support increased lipid synthesis and cell proliferation. Major enzymes required for lipogenesis that have been shown to be up regulated in cancer are Ac-CoA carboxylase 1 (ACACA), fatty acid synthase (FASN) and a few others [48]. However, metabolic enzymes such as MDH1 and malic enzyme 1 (ME1) also help support the conversion of Ac-CoA into lipids through the production of NADPH and pyruvate from malate.

Metabolomics studies using isotope tracers has become a valuable way to deconvolute the complexity of the metabolome and lipidome by measuring the abundances of metabolites in metabolic steady-state or flux. In biochemistry and bioengineering, tracers can help to map pathways, and understand enzyme regulation

and the enhancement/inhibition of yields [50]. Appropriate isotope tracers are chosen based upon the dynamics or activity of the pathway to be evaluated. Previously published metabolomic studies show that tracers such as [U-^{13}C]glucose are useful for evaluating glycolysis, the TCA cycle, and *de novo* serine synthesis, where [1,2-$^{13}C_6$]glucose can be used to evaluate the pentose phosphate pathway (PPP) and others [50]. Here, we used [U-$^{13}C_6$]glucose to evaluate water soluble TCA intermediates and related metabolites. We also employed [4-^{2}H]glucose to assess lipid biosynthesis through sources of NADPH to better understand the consequences of changing the expression of MDH1 *in vitro*.

Metabolic evaluation of MDH1 was conducted using human cell lines. This *in vitro* model was used to harness the comparative power of isogenic controls when determining true differences in cell phenotype, metabolism, and enzymatic reactions caused by changes in expression of MDH1. We acquired a human squamous cell patient line (NCI-H520), a naturally occurring MDH1 amplified adenocarcinoma patient line (NCI-1792), a normal lung epithelial airway cell line (NuLi-1), human embryonic kidney cells (293T), and MDH1 KO 293T cells. To study MDH1 amplification in NCI-H520 cells, a single cell clonal line was created (H520 MDH1^{+}).

In this study, we evaluated the expression of MDH1 in cell lines and assessed the 293T WT and KO cells to determine changes in metabolism and proliferation when MDH1 is lost. We found that increased expression of MDH1 led to increased levels of ME1 in H520 MDH1^{+} cells. Overall, our data indicate that MDH1 is needed for robust proliferation, glucose consumption in metabolism, and lipid biosynthesis.

MATERIALS AND METHODS

Materials

All of the following materials were purchased for the purpose of experimental evaluation of MDH1: Protease inhibitor (Fisher A32959), NADH (Fisher AC271102500), Phenol Red (ATCC PCS-999-001), NCI-H192 (ATCC CRL-5895), ECL Plex goat-α-mouse IgG Cy3 (GE Lifesciences PA43009), PBS (Fisher MT21040CV, Corning 21-031-CM), NCI-H520 (ATCC HTB-182), NuLi-1 (ATCC CRL-4011), Collagen IV (Sigma C7521), C-flag pcDNA3 (Adgene), CellStripper (Corning 25-056-CI), TrypLE (Fisher 12604013), Oxalacetic acid (Fisher AC416600050), MDH1 Protein (Fisher NBP14531501), FBS (VWR 97068-085), 2,2,2-trifluoro-*N*-methylsilyl-acetamide (Machery-Nagel 24589-78-4), chloroform (Sigma 366927), DMEM without glucose and glutamine (Sigma D5030), glucose (Sigma G8270), glutamine (Sigma G8540), hexane (Sigma 34859), norvaline (Sigma N7502), methanol (Sigma 34860), methoxyamine hydrochloride (Supelco 33045-U), *N*-tertbutyldimethylsil-*N*-metylrifluoroacetamide with 1% tert-butyldimetylchlorosilane (Regis Technologies 1-270143-200), pyridine (Sigma 270407), sodium chloride (Sigma S3014), sulfuric acid (Sigma 339741), [$U^{13}C_6$]glucose (Cambridge Isotope Laboratories CLM-1396), and [4-^{2}H]glucose (Omicron Biochemical, Inc. GLC-035).

Transfections and Stable Cell Line Generation

A pcDNA3.1+/C(K)-DYK vector containing a *C*-terminal FLAG tag fused to MDH1 (Genescript) was transfected into NCI-H520 cells using Lipofectamine 3000. Cells expressing the vector were selected for using a concentration of 0.8 mg/mL G418 (Thermo Fisher 087721) for 2 weeks and maintained in half this concentration for the

lifetime of the cell line. Parent lines expressing the vector as confirmed by western were chosen for single cell selection. For selection, $1x10^4$ cells were placed in well A1 of 96-well plate. This well was diluted 1:2 down the first column and then the wells of column 1 were diluted 1:2 across the plate to column 12. After 7-10 days, identified single cell colonies were dissociated and re-diluted 1:2 in a column of a new 96-well plate. Identified single cell colonies were moved to a 24-well plate after 8-12 days, then to a 6-well after 9-22 days, and lastly expanded in a T-75 flask. This monoclonal population was evaluated by western to confirm flag and MDH1 expression levels.

Cell Culture and Isotopic Labeling

The following cell lines were maintained in their respective medias with 10% FBS: HEK 293T WT and MDH1 KO cells utilized DMEM, squamous carcinoma cells NCI-H520 required RPMI ATCC-formulated (ATCC 30-2001) and adenocarcinoma NCI-H1792 used RPMI. Normal epithelial lung cells NuLi-1 cells used airway epithelial cell basal medium (ATCC PCS-300-030) with the bronchial epithelial cell growth kit (ATCC PCS-300-040) additives with no FBS. Cell number was determined using a hemocytometer. For isotopic labeling experiments in 293T cell lines, cells were cultured in 6-well or 12-well plates in glucose- and glutamine- free DMEM at pH 7.4, supplemented with 10% dialyzed Tet-free FBS, 4 mM *L*-glutamine, and 10 or 25 mM of the appropriate deuterated glucose tracer ([4-^{2}H]glucose, Omicron Biochemical, Inc.) or heavy glucose tracer ([U-$^{13}C_6$]glucose, Cambridge Isotope Laboratories, Inc.) for a 24 h incubation.

Cell Proliferation and Rescue Assays

On day 0 (D0), $5x10^5$ cells/well of 293T WT and MDH1 KO cells were seeded in 12-well plates, with 3 plates for each cell type. On D2-D4 cells were counted on a

hemocytometer in biological triplicate. Rescue experiments required the addition of 1 mM sodium pyruvate (Gibco 11360-070) or 1 mM 2-ketobuteric acid (sigma K401-5G) added to the medium.

Metabolite extraction and YSI Secretion Analysis

Polar metabolites and fatty acids were extracted after media removal using methanol/water/chloroform as previously described [51]. 293T WT and MDH1 KO cells were cultured in 6-well or 12-well plates, and volumes of tracer media and extraction buffers were adjusted accordingly. Derivatization of both polar metabolites and fatty acids has been described previously [51]. In short, derivatized samples were analyzed by GC-MS using a DB-35MS column mounted in an Agilent 7890A gas chromatograph (GC) interfaced with an Agilent 5975C mass spectrometer (MS). Mass isotopomer distributions were established by integrating metabolite ion fragments and corrected for natural abundance using algorithms adapted and developed by the Metallo laboratory [52,53]. Extracted media was analyzed in a 96-well plate on the YSI 2950 Biochemical Analyzer to assess secreted protein output.

Isotopomer Spectral Analysis

We followed the isotopomer spectral analysis method used in Lewis et. al [53]. Briefly, the measured palmitate mass isotopomer distribution was compared to a simulated palmitate using a reaction network for the biosynthesis of palmitate using the number of NADPH molecules consumed to form a palmitate molecule [51,53]. Estimated parameters for the relative enrichment of the lipogenic NADPH pool from the [4-^{2}H]glucose tracer and the percentage of *de novo* synthesized fatty acids were extracted from a best-fit model using the isotopomer network compartmental analysis platform with

metabolic flux analysis software package (Fig. S2)[54]. Confidence intervals at 95% for both parameters were estimated by assessing the sensitivity of the sum of squared residuals between quantified and modeled palmitate mass isotopomer distributions to small variations in flux [55].

Protein Extraction and Westerns

Whole-cell extracts were created from cells lysed in RIPA buffer with protease and phosphatase inhibitors. Protein expression was analyzed by western blotting using antibodies against FLAG (DYKDDDDK tag, invitrogen), MDH1 (c-term Abcam ab180152, Novus), ME1 (Fisher MA5-23524), actin (Fisher MA5-15739) and vinculin (Sigma V9131-2ML). All protein lysate concentrations were normalized using a Pierce BCA assay (Fisher PI23228).

Steady-State Kinetics

All enzymatic assays utilized an 8452 diode array spectrophotometer (OLIS, Atlanta, GA). Unknown MDH1 enzymatic concentrations were normalized to 15 µg of total protein from cell lysates and optimized for each cell lysate to ensure optimal signal and linear range. For the conversion of OAA to malate [56,57], the reaction was initiated by adding saturating NADH (200 µM final concentration) and 30 µM OAA in MDH1 assay buffer (10 mM Na/K Phos, pH 7.4 at 37 °C). The change in absorbance due to NADH depletion was monitored at 340 nm. For this reaction, the slope of the linear range of the incubations were calculated and converted to nM NADPH using the molar extinction coefficient for NADH of 6.22 cm^{-1} mM^{-1} to obtain a hypothetical "k_{obs}" (i.e. nM NADPH/µg protein at 30µM substrate). Assays were performed with at least three lysate preparations.

RESULTS

MDH1 successfully amplified in squamous NSCLC cell line

To create a cellular tool to evaluate the effect of MDH1 expression in squamous carcinoma NSCLCs, NCI-H520 cells (WT H520) were transfected with a pcDNA3.1 amplification vector with MDH1 fused to a *C*-terminal FLAG tag (MDH1 vector, Fig. 1b). H520 parent lines resulting from transfection of the MDH1 vector were screened for FLAG expression and clonally single cell selected (Fig. 1c). Levels of MDH1 and FLAG expression varied between clones based upon immunoblot analysis, therefore the highest expressors of MDH1 and FLAG were later evaluated by kinetics as a second screen (Fig. 1d). A Michaelis-Menten-like plot was generated to determine an appropriate OAA concentration using the WT H520 cell line for later comparison of MDH1 activity amongst cell lines (Fig. 2a). Since enzyme concentration was unknown, we do not report the Michaelis-Menten parameters k_{cat} and K_m, and instead report k_{obs} values. We used steady-state kinetics assays to identify the clone (H520 MDH1$^+$) with the highest rates of malate production by the lysates as compared to the parental WT H520 cell line (Fig. 2b).

H1792 adenocarcinoma cells express the highest levels of MDH1

To determine the baseline expression of our MDH1 amplified and WT cell lines, we used steady-state kinetics experiments with cell lysates. Direct comparison of k_{obs} values for normal lung (NuLi-1), WT H520, H520 MDH1$^+$, and the naturally MDH1 amplified adenocarcinoma NSCLC (H1792) cells revealed that the H1792 cells had the highest MDH1 activity followed by the H520 MDH1$^+$ cells (Fig. 2b).

MDH1 KO cell line partially rescued by metabolites

We acquired readily available WT and MDH1 KO cells in a 293T background, and noted a substantial difference in proliferation rate between the WT and MDH1 KO cell lines (Fig. 3a). We then sought to determine if the growth defect could be rescued by metabolite intermediates, and thus we tested supplementing the KO cells with pyruvate and α-ketobutyric acid. Pyruvate directly bypasses the loss of MDH1 by entering the mitochondria to supplement the TCA cycle with OAA after conversion by pyruvate carboxylase (Fig. 4c). Once transported into the mitochondria, α-ketobutyric acid is converted into succinyl-CoA by a series of 4 mitochondrial enzymes leading to the generation of malate from fumarate to increase TCA cycling. Both compounds facilitated a partial rescue in growth that was significantly apparent by day 4 (Fig. 3c). Supplementation of these compounds on WT cells showed no difference in growth rates (Fig. 3b).

Loss of MDH1 decreases TCA cycling, lactate secretion, and lipid biosynthesis

We then performed metabolomic studies to probe the effects caused by MDH1 loss in the MDH1 KO cells. Evaluation of metabolomics with tracers has been used previously to trace metabolites in the cytosol and mitochondria of cells [53]. Using a [$U^{13}C_6$]-glucose tracer and GC-MS, we identified differences in the abundance of metabolite intermediates between the WT and MDH1 KO cells. Initially, we found that the percentage of labeling and the normalized abundance from the glucose tracer was decreased in the MDH1 KO cells compared to WT (Fig. 4a, b). All TCA intermediates were decreased except for aspartate. This metabolite may be increased due to the loss of MDH1 in the malate-aspartate shuttle (Fig. 4b). When we evaluated the levels of secreted metabolites using YSI, there was only a detected decrease in lactate secretion

by the MDH1 KO cells (Fig. 4d), indicating a shift in how glucose is utilized [49]. Since the majority of intermediates created down stream of glucose are down, this suggests that the demand for glucose is also down or it is being used differently in the MDH1 KO cells.

To evaluate lipogenesis, a [4-^{2}H]-glucose tracer and GC-MS were used. [4-^{2}H]-glucose has previously been used to label the NADPH pool created in glycolysis via the transport of the deuterated hydrogen from carbon 4 of the glucose tracer to NADP(H) [50,53]. When the deuterated NADP(H) is converted to NAD^{+}, the heavy hydrogen is incorporated into the formed product, facilitating tracking of synthesized intermediates containing that deuterated hydrogen (Fig 5a). This is an ideal way to monitor changes in MDH1 activity since MDH1 uses NADH to produce malate and NAD^{+}. This malate in turn serves as a substrate for ME1, which catalyzes an $NADP^{+}$-dependent conversion of malate to pyruvate and NADPH. This NADPH in part helps support lipid biosynthesis. Thus, palmitate was analyzed as a lipid proxy using ISA analysis to determine the percentage of labeling from the heavy glucose tracer. We found that labeling of palmitate in MDH1 KO cells was attenuated (Fig. 5b). The contribution of heavy glucose to the lipogenic pool of AcCoA and the percentage of newly synthesized palmitate was found to be significantly decreased (Fig. 5c).

ME1 expression is enhanced in MDH1 amplified cells

Upon finding that the loss of MDH1 activity led to decreased TCA cycling and lipid biosynthesis, we examined relative expression levels of enzymes that support lipogenesis in conjunction with MDH1, such as ME1. We compared ME1 expression levels between NuLi-1, WT H520, H520 $MDH1^{+}$, and H1792 cells, and showed that ME1 expression is 9-fold higher than normal lung cells in the H520 $MDH1^{+}$ cells, 6-fold higher in WT H520

cells, and 3-fold in H1792 cells (Fig. 6b). When compared to WT H520 cells, ME1 expression in H520 MDH1^{+} cells were only slightly higher (~0.5-fold, Fig. 6b).

DISCUSSION

Here, we used an *in vitro* human cell model system to evaluate changes in MDH1 expression. We found that KO of MDH1 decreases proliferation, TCA cycling, lactate secretion, and lipogenesis. Previously Hanse et. al. showed that KO of MDH1 in Jurkat T-cells have a proliferation defect [46]. Our data from the MDH1 KO 293T cells confirms this finding and shows consistency between results. Our data also supports the finding that glucose utilization is decreased in the MDH1 KO 293T cells as indicated by lowered abundance of TCA intermediates. We partially rescued MDH1 KO 293T cells with pyruvate and α-ketobutyric acid, consistent with previous pyruvate rescue of MDH1 KO Jurkat cells [46]. According to Hanse et al., when MDH1 KO Jurkat cells were engineered to re-express MDH1, the proliferation defect was also rescued [46]. Currently, we do not have a paired amplified and KO MDH1 cell line, however in our $MDH1^+$ H520 cells we observed a decrease in cell proliferation compared to H520 WT cells. This may indicate that excess of MDH1 may not always support cell proliferation as predicted. However, we observed that increased MDH1 in the H520 $MDH1^+$ cells led to amplified ME1 expression, allowing for the potential of an increase in CO_2, pyruvate, and NADPH equivalents. It would be interesting to assess the metabolism of the H520 WT and H520 $MDH1^+$ cells to better understand if increased ME1 also translates to increased lipogenesis, regardless of the decrease observed in proliferation.

Interesting future experiments would be to evaluate the differences in metabolism between squamous and adenocarcinoma cell lines. H520 $MDH1^+$ and H1792 cells showed differences in MDH1 kinetic activity, expression of ME1, and proliferation rates that future metabolic tracing may shed light on. Squamous cells also express high levels

of GLUT1 compared to adenocarcinoma cells, revealing their addiction to glucose [49], so these will be important future avenues to explore. Evaluating serine metabolism in both NSCLC cell types may also be advantageous, since serine can lead to the production of pyruvate after breakdown (Fig. 5a) and is a precursor of sphingolipids and the headgroup precursor for phospholipids that are used in membranes and may support proliferation [58]. Preliminarily, we found by YSI that the serine levels of the MDH1 KO cells decrease by ~50% when no serine is in the media compared to when it is added (data not shown). Identifying that MDH1 KO 293T cells transport serine from the extracellular environment, however it has been shown that some cancer cells *de novo* synthesize serine from glucose indicating that serine may have a distinct role in cancer cells [58]. Determination of a serine synthesis dependency in MDH1 amplified NSCLCs and evaluation of if *de novo* synthesis of serine is utilized differently in these cells than serine imported from the environment is an avenue to be explored.

In short, we used human cells to evaluate changes in MDH1 expression. We found that we could successfully increase MDH1 expression in H520 WT cells to create a valuable tool to study MDH1 amplification in NSCLC. Among our models, H1792 cells had the highest MDH1 expression and MDH1 activity, and also led to amplification of ME1 expression. KO of MDH1 revealed that proliferation, TCA cycling, lactate secretion, and lipogenesis are all decreased. Overall, this study supports the idea that MDH1 is important for metabolism and lipid synthesis in normal and NSCLC cells.

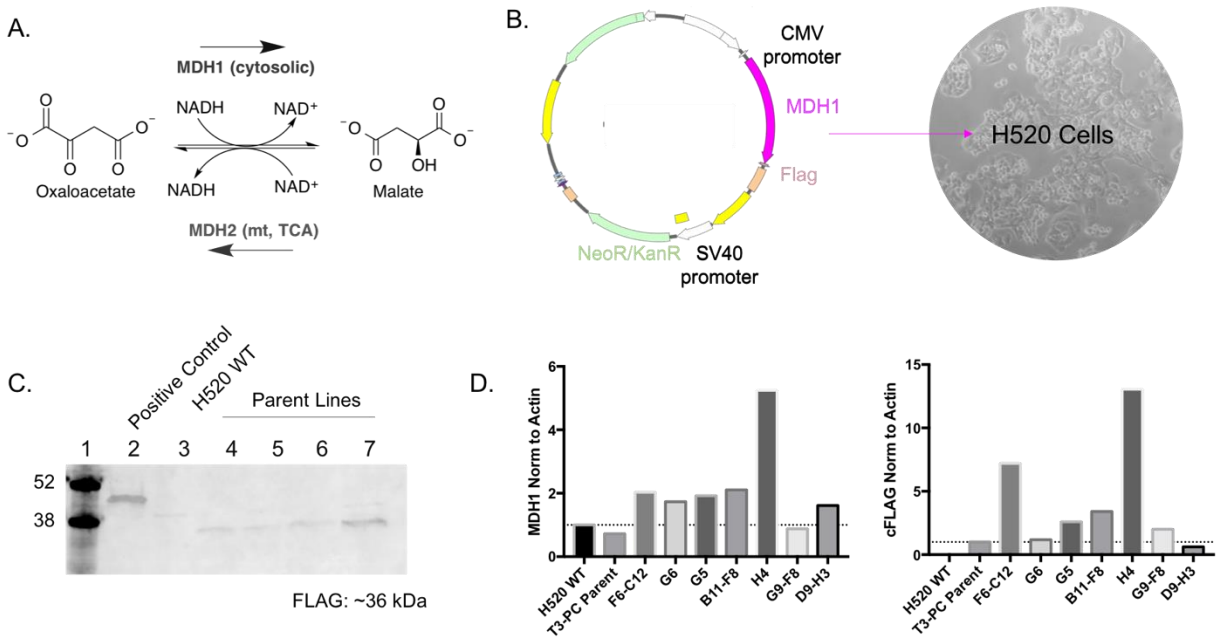

Figure 2.5: H520 MDH1^{+} cells successfully created from H520 WT cells

(A) MDH1 and MDH2 enzymatic reactions. (B) MDH1 amplification vector showing the fusion of MDH1 and FLAG transfected into H520 WT cells. (C) Verification of FLAG expression by western in H520 WT and MDH1 parental lines. (D) Variable expression of MDH1 and FLAG found in the H520 clonal lines.

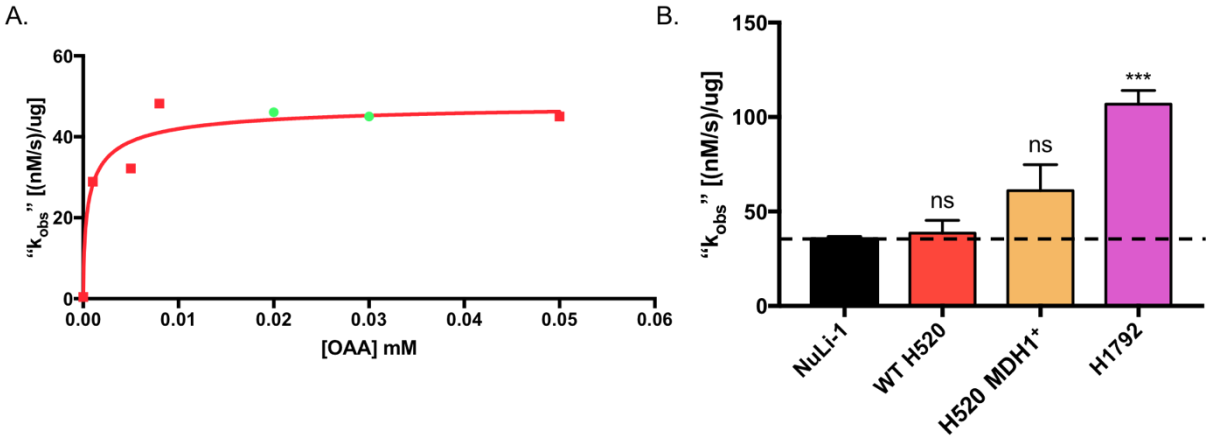

Figure 2.6: Kinetic evaluation of MDH1 expression in lung cells

(A) Michaelis Menten like plot created using WT H520 "k_{obs}" values. Green dots indicate steady concentrations that can be used to compare the MDH1 rate from multiple cell lines. (B) Comparison of "k_{obs}" values at a concentration of 0.03 mM OAA for normal lung (NULi-1), squamous NSCLC (H520 WT), MDH1 amplified squamous NSCLC (H520 MDH1^{+}), and adenocarcinoma NSCLC (H1792) cells.

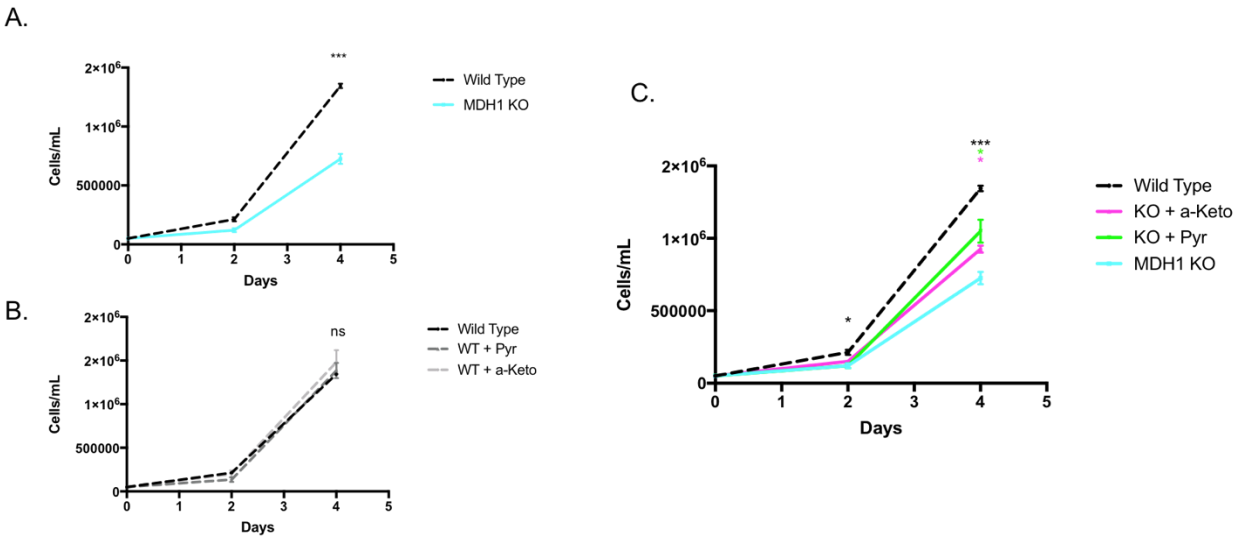

Figure 2.7: MDH1 KO cells partially rescued by pyruvate and α-ketobutyric acid

(A) Growth of wild type and MDH1 KO 293T cells over 4 days. (B) Comparison of WT 293T cells with no treatment, treatment with 1 mM pyruvate, and treatment with 1 mM α-ketobutyric acid. (C) Partial rescue of 293T MDH1 KO cells by 1 mM pyruvate and 1 mM α-ketobutyric acid compared to no treatment and the WT control with significance calculated using the student's T test (* $p < 0.01$, *** $p < 0.0001$).

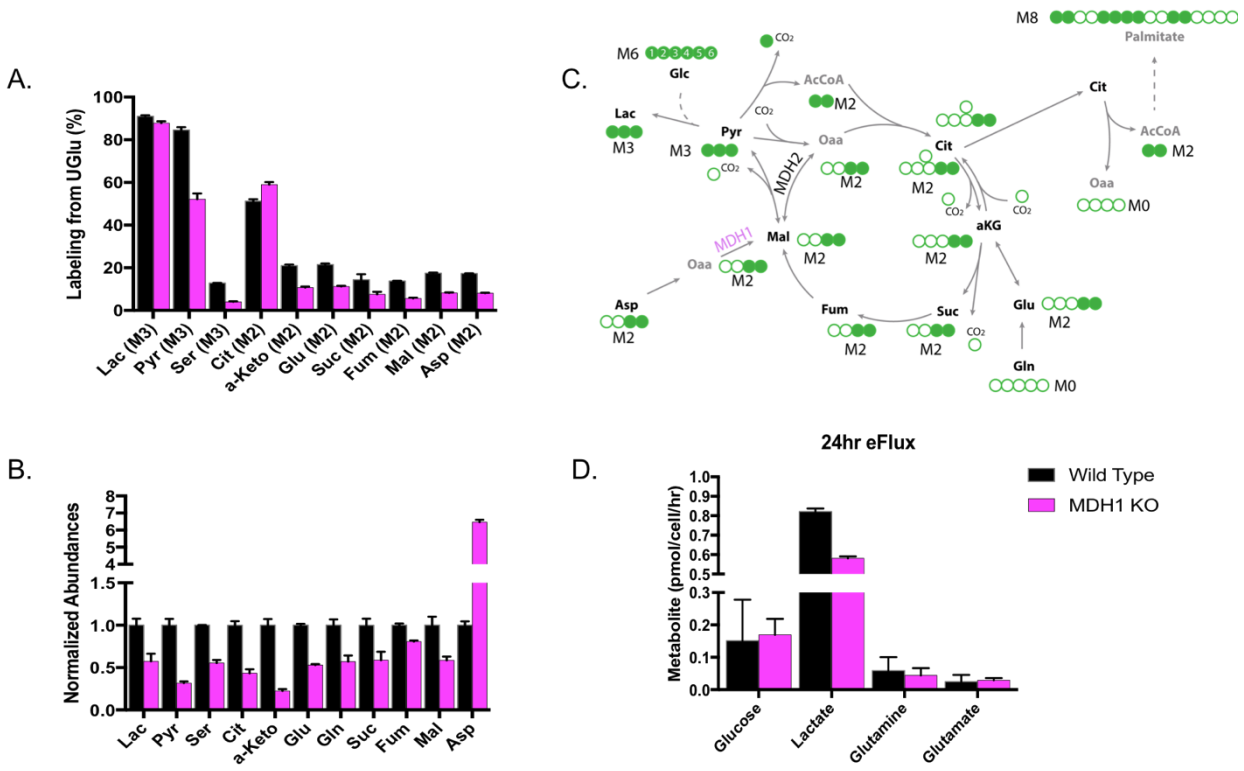

Figure 2.8: [$U^{13}C_6$]glucose tracing reveals decreased TCA cycling and lactate secretion

293T WT and MDH1 KO cells were incubated in [$U^{13}C_6$]glucose tracer media for 24 h. (A) Differential amounts of label from labelled glucose was incorporated into TCA intermediates and the (B) abundances of label normalized to internal controls and cell numbers revealed attenuated TCA cycling and a buildup of aspartate (Asp) in MDH1 KO cells. (C) A metabolism map tracing the use of heavy glucose labeling through glycolysis, the TCA cycle and lipid synthesis. (D) Secreted metabolites glucose (Glc), lactate (Lac), glutamine (Gln), and glutamate (Glu) were evaluated using YSI.

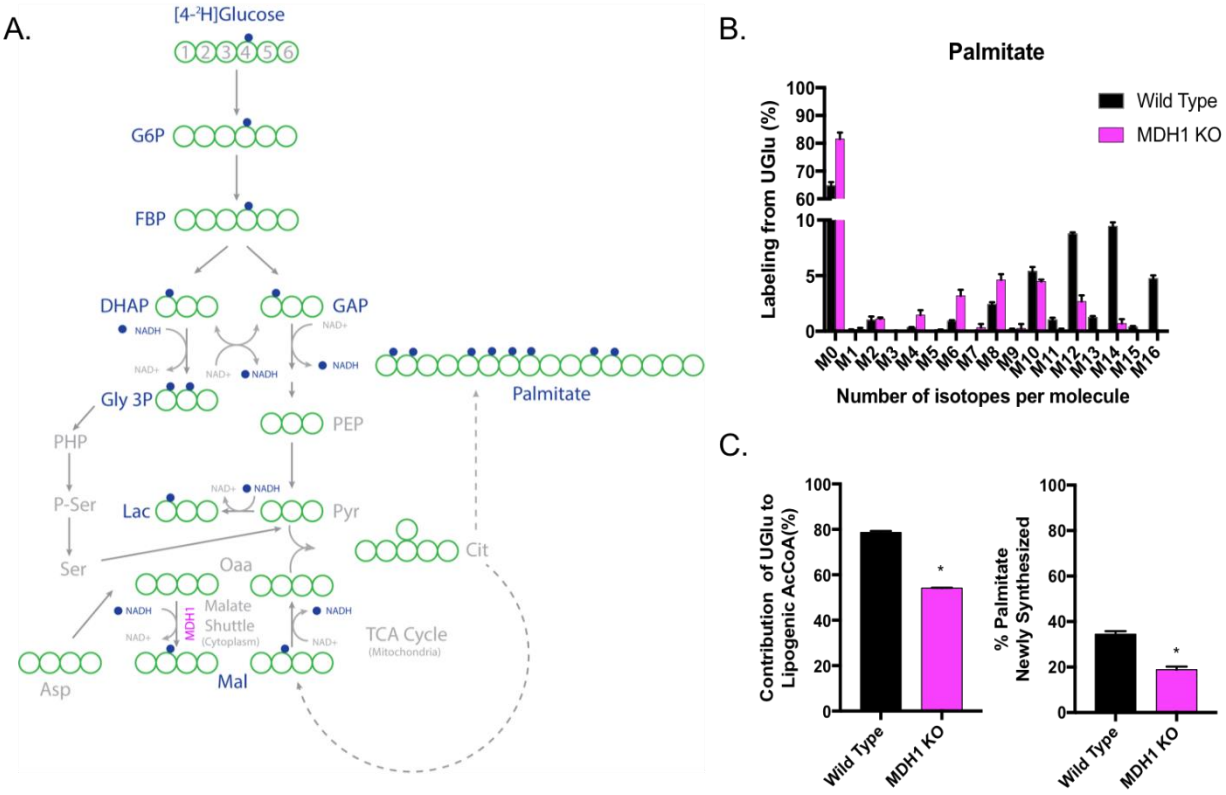

Figure 2.9: [4-^{2}H]glucose tracer reveals decreased lipogenesis

(A) Metabolism map tracing the use of heavy glucose labeling through glycolysis, the TCA cycle and lipid synthesis. (B) Palmitate synthesis is down in the MDH1 KO cells as indicated by decreased glucose label, total palmitate derived from labelled glucose and the total calculated amount of newly synthesized palmitate with error bars, 95% confidence intervals and S.E.M. (n = 3) with * $p < 0.05$.

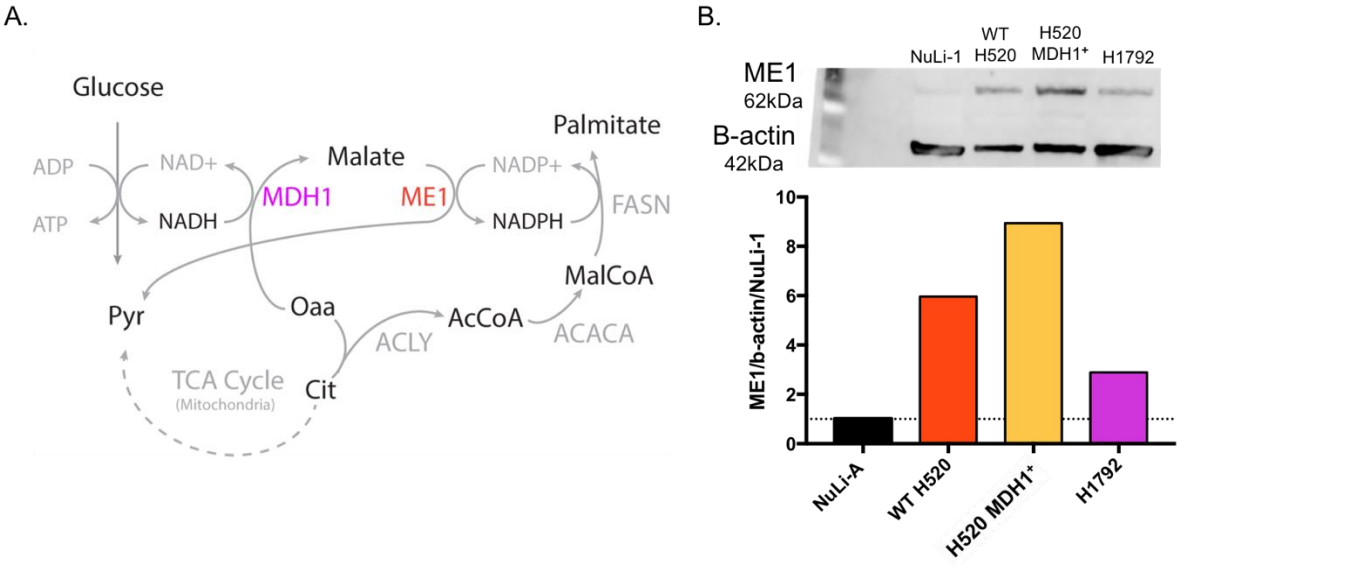

Figure 2.10: ME1 is increased in MDH1 amplified cells

(A) Metabolism map following glucose through glycolysis, the TCA cycle and lipid synthesis with an emphasis on the MDH1 and ME1 enzymatic team supporting lipogenesis. (B) Measured expression of ME1 normalized to β-actin in normal lung (NULi-1), squamous NSCLC (H520 WT), MDH1 amplified squamous NSCLC (H520 MDH1^{+}), and adenocarcinoma NSCLC (H1792) cells.

REFERENCES

[1] Xu, X., Zhao, J., Xu, Z., Peng, B., Huang, Q., Arnold, E. and Ding, J. (2004). Structures of Human Cytosolic NADP-dependent Isocitrate Dehydrogenase Reveal a Novel Self-regulatory Mechanism of Activity. Journal of Biological Chemistry 279, 33946-33957.

[2] Rendina, A.R., Pietrak, B., Smallwood, A., Zhao, H., Qi, H., Quinn, C., Adams, N.D., Concha, N., Duraiswami, C., Thrall, S.H., Sweitzer, S. and Schwartz, B. (2013). Mutant IDH1 enhances the production of 2-hydroxyglutarate due to its kinetic mechanism. Biochemistry 52, 4563-77.

[3] Dang, L., Yen, K. and Attar, E.C. (2016). IDH mutations in cancer and progress toward development of targeted therapeutics. Ann Oncol 27, 599-608.

[4] Yan, H., Parsons, D.W., Jin, G., McLendon, R., Rasheed, B.A., Yuan, W., Kos, I., Batinic-Haberle, I., Jones, S., Riggins, G.J., Friedman, H., Friedman, A., Reardon, D., Herndon, J., Kinzler, K.W., Velculescu, V.E., Vogelstein, B. and Bigner, D.D. (2009). IDH1 and IDH2 mutations in gliomas. N Engl J Med 360, 765-73.

[5] Avellaneda Matteo, D., Grunseth, A.J., Gonzalez, E.R., Anselmo, S.L., Kennedy, M.A., Moman, P., Scott, D.A., Hoang, A. and Sohl, C.D. (2017). Molecular mechanisms of isocitrate dehydrogenase 1 (IDH1) mutations identified in tumors: The role of size and hydrophobicity at residue 132 on catalytic efficiency. J Biol Chem 292, 7971-7983.

[6] Mu, L., Long, Y., Yang, C., Jin, L., Tao, H., Ge, H., Chang, Y.E., Karachi, A., Kubilis, P.S., De Leon, G., Qi, J., Sayour, E.J., Mitchell, D.A., Lin, Z. and Huang, J. (2018). The IDH1 Mutation-Induced Oncometabolite, 2-Hydroxyglutarate, May Affect DNA Methylation and Expression of PD-L1 in Gliomas. Front Mol Neurosci 11, 82.

[7] Wang, P., Wu, J., Ma, S., Zhang, L., Yao, J., Hoadley, K.A., Wilkerson, M.D., Perou, C.M., Guan, K.L., Ye, D. and Xiong, Y. (2015). Oncometabolite D-2-hydroxyglutarate inhibits ALKBH DNA repair enzymes and sensitizes IDH mutant cells to alkylating agents. Cell Rep 13, 2353-61.

[8] Dhillon, S. (2018). Ivosidenib: First Global Approval. Drugs 78, 1509-1516.

[9] Calvert, A.E., Chalastanis, A., Wu, Y., Hurley, L.A., Kouri, F.M., Bi, Y., Kachman, M., May, J.L., Bartom, E., Hua, Y., Mishra, R.K., Schiltz, G.E., Dubrovskyi, O.,

Mazar, A.P., Peter, M.E., Zheng, H., James, C.D., Burant, C.F., Chandel, N.S., Davuluri, R.V., Horbinski, C. and Stegh, A.H. (2017). Cancer-associated IDH1 promotes growth and resistance to targeted therapies in the absence of mutation. Cell Rep 19, 1858-1873.

[10] Gao, J., Aksoy, B.A., Dogrusoz, U., Dresdner, G., Gross, B., Sumer, S.O., Sun, Y., Jacobsen, A., Sinha, R., Larsson, E., Cerami, E., Sander, C. and Schultz, N. (2013). Integrative analysis of complex cancer genomics and clinical profiles using the cBioPortal. Science signaling 6, pl1-pl1.

[11] Cerami, E., Gao, J., Dogrusoz, U., Gross, B.E., Sumer, S.O., Aksoy, B.A., Jacobsen, A., Byrne, C.J., Heuer, M.L., Larsson, E., Antipin, Y., Reva, B., Goldberg, A.P., Sander, C. and Schultz, N. (2012). The cBio cancer genomics portal: an open platform for exploring multidimensional cancer genomics data. Cancer discovery 2, 401-404.

[12] Dang, L., White, D.W., Gross, S., Bennett, B.D., Bittinger, M.A., Driggers, E.M., Fantin, V.R., Jang, H.G., Jin, S., Keenan, M.C., Marks, K.M., Prins, R.M., Ward, P.S., Yen, K.E., Liau, L.M., Rabinowitz, J.D., Cantley, L.C., Thompson, C.B., Vander Heiden, M.G. and Su, S.M. (2009). Cancer-associated IDH1 mutations produce 2-hydroxyglutarate. Nature 462, 739-44.

[13] Tönjes, M. et al. (2013). BCAT1 promotes cell proliferation through amino acid catabolism in gliomas carrying wild-type IDH1. Nature medicine 19, 901-908.

[14] Zhu, H., Zhang, Y., Chen, J., Qiu, J., Huang, K., Wu, M. and Xia, C. (2017). IDH1 R132H mutation enhances cell migration by activating AKT-mTOR signaling pathway, but sensitizes cells to 5-FU treatment as NADPH and GSH are reduced. PLoS One 12, e0169038.

[15] Hurley, J.H., Dean, A.M., Sohl, J.L., Koshland, D.E. and Stroud, R.M. (1990). Regulation of an Enzyme by Phosphorylation at the Active Site. Science 249, 1012-1016.

[16] Lin, A.P. and McAlister-Henn, L. (2003). Homologous binding sites in yeast isocitrate dehydrogenase for cofactor (NAD+) and allosteric activator (AMP). J Biol Chem 278, 12864-72.

[17] Reitman, Z.J. and Yan, H. (2010). Isocitrate dehydrogenase 1 and 2 mutations in cancer: alterations at a crossroads of cellular metabolism. Journal of the National Cancer Institute 102, 932-941.

[18] Chen, D., Xia, S., Wang, M., Lin, R., Li, Y., Mao, H., Aguiar, M., Famulare, C.A., Shih, A.H., Brennan, C.W., Gao, X., Pan, Y., Liu, S., Fan, J., Jin, L., Song, L., Zhou, A., Mukherjee, J., Pieper, R.O., Mishra, A., Peng, J., Arellano, M., Blum, W.G., Lonial, S., Boggon, T.J., Levine, R.L. and Chen, J. (2019). Mutant and Wild-Type Isocitrate Dehydrogenase 1 Share Enhancing Mechanisms Involving Distinct Tyrosine Kinase Cascades in Cancer. Cancer Discov 9, 756-777.

[19] Baeza, J., Smallegan, M.J. and Denu, J.M. (2015). Site-specific reactivity of nonenzymatic lysine acetylation. ACS Chem Biol 10, 122-8.

[20] Kim, S.C., Sprung, R., Chen, Y., Xu, Y., Ball, H., Pei, J., Cheng, T., Kho, Y., Xiao, H., Xiao, L., Grishin, N.V., White, M., Yang, X.J. and Zhao, Y. (2006). Substrate and functional diversity of lysine acetylation revealed by a proteomics survey. Mol Cell 23, 607-18.

[21] Mattagajasingh, I., Kim, C.S., Naqvi, A., Yamamori, T., Hoffman, T.A., Jung, S.B., DeRicco, J., Kasuno, K. and Irani, K. (2007). SIRT1 promotes endothelium-dependent vascular relaxation by activating endothelial nitric oxide synthase. Proc Natl Acad Sci U S A 104, 14855-60.

[22] Lombard, D.B., Alt, F.W., Cheng, H.L., Bunkenborg, J., Streeper, R.S., Mostoslavsky, R., Kim, J., Yancopoulos, G., Valenzuela, D., Murphy, A., Yang, Y., Chen, Y., Hirschey, M.D., Bronson, R.T., Haigis, M., Guarente, L.P., Farese, R.V., Jr., Weissman, S., Verdin, E. and Schwer, B. (2007). Mammalian Sir2 homolog SIRT3 regulates global mitochondrial lysine acetylation. Mol Cell Biol 27, 8807-14.

[23] Starai, V.J., Celic, I., Cole, R.N., Boeke, J.D. and Escalante-Semerena, J.C. (2002). Sir2-dependent activation of acetyl-CoA synthetase by deacetylation of active lysine. Science 298, 2390-2.

[24] Sadoul, K., Wang, J., Diagouraga, B. and Khochbin, S. (2011). The tale of protein lysine acetylation in the cytoplasm. J Biomed Biotechnol 2011, 970382.

[25] Zhao, S., Xu, W., Jiang, W., Yu, W., Lin, Y., Zhang, T., Yao, J., Zhou, L., Zeng, Y., Li, H., Li, Y., Shi, J., An, W., Hancock, S.M., He, F., Qin, L., Chin, J., Yang, P., Chen, X., Lei, Q., Xiong, Y. and Guan, K.-L. (2010). Regulation of cellular metabolism by protein lysine acetylation. Science (New York, N.Y.) 327, 1000-1004.

[26] Drazic, A., Myklebust, L.M., Ree, R. and Arnesen, T. (2016). The world of protein acetylation. Biochim Biophys Acta 1864, 1372-401.

[27] Yu, W., Dittenhafer-Reed, K.E. and Denu, J.M. (2012). SIRT3 protein deacetylates isocitrate dehydrogenase 2 (IDH2) and regulates mitochondrial redox status. J Biol Chem 287, 14078-86.

[28] Xu, Y., Liu, L., Nakamura, A., Someya, S., Miyakawa, T. and Tanokura, M. (2017). Studies on the regulatory mechanism of isocitrate dehydrogenase 2 using acetylation mimics. Sci Rep 7, 9785.

[29] Hornbeck, P.V., Kornhauser, J.M., Tkachev, S., Zhang, B., Skrzypek, E., Murray, B., Latham, V. and Sullivan, M. (2012). PhosphoSitePlus: a comprehensive resource for investigating the structure and function of experimentally determined post-translational modifications in man and mouse. Nucleic Acids Research 40, D261-D270.

[30] Rardin, M.J., Newman, J.C., Held, J.M., Cusack, M.P., Sorensen, D.J., Li, B., Schilling, B., Mooney, S.D., Kahn, C.R., Verdin, E. and Gibson, B.W. (2013). Label-free quantitative proteomics of the lysine acetylome in mitochondria identifies substrates of SIRT3 in metabolic pathways. Proc Natl Acad Sci U S A 110, 6601-6.

[31] Beli, P., Lukashchuk, N., Wagner, S.A., Weinert, B.T., Olsen, J.V., Baskcomb, L., Mann, M., Jackson, S.P. and Choudhary, C. (2012). Proteomic investigations reveal a role for RNA processing factor THRAP3 in the DNA damage response. Molecular cell 46, 212-225.

[32] Avellaneda Matteo, D., Wells, G.A., Luna, L.A., Grunseth, A.J., Zagnitko, O., Scott, D.A., Hoang, A., Luthra, A., Swairjo, M.A., Schiffer, J.M. and Sohl, C.D. (2018). Inhibitor potency varies widely among tumor-relevant human isocitrate dehydrogenase 1 mutants. Biochem J 475, 3221-3238.

[33] The UniProt, C. (2018). UniProt: a worldwide hub of protein knowledge. Nucleic Acids Research 47, D506-D515.

[34] Shi, D., Morizono, H., Yu, X., Tong, L., Allewell, N.M. and Tuchman, M. (2001). Human ornithine transcarbamylase: crystallographic insights into substrate recognition and conformational changes. The Biochemical journal 354, 501-509.

[35] Xiong, Y. and Guan, K.-L. (2012). Mechanistic insights into the regulation of metabolic enzymes by acetylation. The Journal of cell biology 198, 155-164.

[36] Yu, W., Lin, Y., Yao, J., Huang, W., Lei, Q., Xiong, Y., Zhao, S. and Guan, K.-L. (2009). Lysine 88 acetylation negatively regulates ornithine carbamoyltransferase activity in response to nutrient signals. The Journal of biological chemistry 284, 13669-13675.

[37] Qiu, X., Brown, K., Hirschey, M.D., Verdin, E. and Chen, D. (2010). Calorie restriction reduces oxidative stress by SIRT3-mediated SOD2 activation. Cell Metab 12, 662-7.

[38] Wang, M.-M., You, D. and Ye, B.-C. (2017). Site-specific and kinetic characterization of enzymatic and nonenzymatic protein acetylation in bacteria. Scientific reports 7, 14790-14790.

[39] Fu, M., Rao, M., Wang, C., Sakamaki, T., Wang, J., Di Vizio, D., Zhang, X., Albanese, C., Balk, S., Chang, C., Fan, S., Rosen, E., Palvimo, J.J., Jänne, O.A., Muratoglu, S., Avantaggiati, M.L. and Pestell, R.G. (2003). Acetylation of Androgen Receptor Enhances Coactivator Binding and Promotes Prostate Cancer Cell Growth. Molecular and Cellular Biology 23, 8563-8575.

[40] White, R.H., Keberlein, M. and Jackson, V. (2012). A Mutational Mimic Analysis of Histone H3 Post-Translational Modifications: Specific Sites Influence the Conformational State of H3/H4, Causing either Positive or Negative Supercoiling of DNA. Biochemistry 51, 8173-8188.

[41] Wang, X., Hu, S. and Liu, L. (2017). Phosphorylation and acetylation modifications of FOXO3a: Independently or synergistically? Oncology letters 13, 2867-2872.

[42] Fan, J., Krautkramer, K.A., Feldman, J.L. and Denu, J.M. (2015). Metabolic regulation of histone post-translational modifications. ACS chemical biology 10, 95-108.

[43] Neumann, H., Peak-Chew, S.Y. and Chin, J.W. (2008). Genetically encoding Nε-acetyllysine in recombinant proteins. Nature Chemical Biology 4, 232-234.

[44] Wang, B., Ye, Y., Yang, X., Liu, B., Wang, Z., Chen, S., Jiang, K., Zhang, W., Jiang, H., Mustonen, H., Puolakkainen, P., Wang, S., Luo, J. and Shen, Z. (2020). SIRT2-dependent IDH1 deacetylation inhibits colorectal cancer and liver metastases. EMBO reports n/a, e48183.

[45] Mohamed, A., Deng, X., Khuri, F.R. and Owonikoko, T.K. (2014). Altered glutamine metabolism and therapeutic opportunities for lung cancer. Clin Lung Cancer 15, 7-15.

[46] Hanse, E.A., Ruan, C., Kachman, M., Wang, D., Lowman, X.H. and Kelekar, A. (2017). Cytosolic malate dehydrogenase activity helps support glycolysis in actively proliferating cells and cancer. Oncogene 36, 3915-3924.

[47] Levine, A.J. and Puzio-Kuter, A.M. (2010). The control of the metabolic switch in cancers by oncogenes and tumor suppressor genes. Science 330, 1340-4.

[48] Cheng, C., Geng, F., Cheng, X. and Guo, D. (2018). Lipid metabolism reprogramming and its potential targets in cancer. Cancer Communications 38, 27.

[49] Goodwin, J., Neugent, M.L., Lee, S.Y., Choe, J.H., Choi, H., Jenkins, D.M.R., Ruthenborg, R.J., Robinson, M.W., Jeong, J.Y., Wake, M., Abe, H., Takeda, N., Endo, H., Inoue, M., Xuan, Z., Yoo, H., Chen, M., Ahn, J.-M., Minna, J.D., Helke, K.L., Singh, P.K., Shackelford, D.B. and Kim, J.-w. (2017). The distinct metabolic phenotype of lung squamous cell carcinoma defines selective vulnerability to glycolytic inhibition. Nature Communications 8, 15503.

[50] Jang, C., Chen, L. and Rabinowitz, J.D. (2018). Metabolomics and Isotope Tracing. Cell 173, 822-837.

[51] Metallo, C.M., Gameiro, P.A., Bell, E.L., Mattaini, K.R., Yang, J., Hiller, K., Jewell, C.M., Johnson, Z.R., Irvine, D.J., Guarente, L., Kelleher, J.K., Vander Heiden, M.G., Iliopoulos, O. and Stephanopoulos, G. (2012). Reductive glutamine metabolism by IDH1 mediates lipogenesis under hypoxia. Nature 481, 380-4.

[52] Fernandez, C.A., Des Rosiers, C., Previs, S.F., David, F. and Brunengraber, H. (1996). Correction of 13C Mass Isotopomer Distributions for Natural Stable Isotope Abundance. Journal of Mass Spectrometry 31, 255-262.

[53] Lewis, C.A., Parker, S.J., Fiske, B.P., McCloskey, D., Gui, D.Y., Green, C.R., Vokes, N.I., Feist, A.M., Vander Heiden, M.G. and Metallo, C.M. (2014). Tracing compartmentalized NADPH metabolism in the cytosol and mitochondria of mammalian cells. Mol Cell 55, 253-63.

[54] Young, J.D. (2014). INCA: a computational platform for isotopically non-stationary metabolic flux analysis. Bioinformatics 30, 1333-5.

[55] Antoniewicz, M.R., Kelleher, J.K. and Stephanopoulos, G. (2006). Determination of confidence intervals of metabolic fluxes estimated from stable isotope measurements. Metabolic Engineering 8, 324-337.

[56] Lee, S.M., Kim, J.H., Cho, E.J. and Youn, H.D. (2009). A nucleocytoplasmic malate dehydrogenase regulates p53 transcriptional activity in response to metabolic stress. Cell Death & Differentiation 16, 738-748.

[57] Lee, S.-M., Dho, S.H., Ju, S.-K., Maeng, J.-S., Kim, J.-Y. and Kwon, K.-S. (2012). Cytosolic malate dehydrogenase regulates senescence in human fibroblasts. Biogerontology 13, 525-536.

[58] Mattaini, K.R., Sullivan, M.R. and Vander Heiden, M.G. (2016). The importance of serine metabolism in cancer. J Cell Biol 214, 249-57.